








Article

Nitrosyl/Diphenylphosphine/Amino Acid–Ruthenium Complexes as Inhibitors of MDA-MB-231 Breast Cancer Cells

Marília I. F. Barbosa ¹, Rodrigo S. Corrêa ², Adriana P. M. Guedes ³, Alex M. Graça ³, Franciyelli M. Andrade ⁴,
Celisnólia M. Leite ³, Elisângela P. Silveira-Lacerda ⁴, Javier Ellena ⁵, Henrique V. Reis ¹,
Antônio C. Doriguetto ¹ and Alzir A. Batista ^{3,*}

¹ Instituto de Química, Universidade Federal de Alfenas, Alfenas 37130-000, MG, Brazil
² Departamento de Química, Universidade Federal de Ouro Preto, Ouro Preto 35400-000, MG, Brazil
³ Departamento de Química, Universidade Federal de São Carlos, São Carlos 13565-905, SP, Brazil; contatomarchezini@gmail.com (A.M.G.)
⁴ Laboratório de Genética Molecular e Citogenética, Instituto de Ciências Biológicas, Universidade Federal de Goiás, Goiânia 74690-900, GO, Brazil
⁵ Instituto de Física de São Carlos, Universidade de São Paulo, São Carlos 13560-970, SP, Brazil
* Correspondence: daab@ufscar.br; Tel.: +55-16-3351-8285

Abstract: Herein, we report on the synthesis and characterization of ruthenium compounds with the general formula $[RuCl(AA-H)(NO)(dppb)PF_6]$, where AA = glycine (1), L-alanine (2), L-phenylalanine (3) and L-valine (4), and dppb = 1,4-bis(diphenylphosphine)butane. The complexes were characterized using elemental analysis, UV/Vis and infrared spectroscopies, ¹H, ¹³C, ³¹P NMR techniques, and cyclic voltammetry. Furthermore, the structures of the compounds (1) and (3) were determined using single-crystal X-ray diffraction. In vitro evaluation of the Ru(II)/nitrosyl/amino acid complexes revealed their cytotoxic activities against triple-negative MDA-MB-231 breast cancer cells, and against the non-tumor murine fibroblast cells. All the compounds decreased the percentage of viable cells, inducing cell death by apoptosis. Additionally, the Ru(II) complexes inhibited the migration of MDA-MB-231 cells at concentrations lower than 35 μM, after 48 h of exposure. Thus, these complexes may be promising agents for the treatment of triple-negative MDA-MB-231 breast cancer.

Keywords: ruthenium; diphenylphosphine; amino acids; nitric oxide; breast cancer cells



Citation: Barbosa, M.I.F.; Corrêa, R.S.; Guedes, A.P.M.; Graça, A.M.; Andrade, F.M.; Leite, C.M.; Silveira-Lacerda, E.P.; Ellena, J.; Reis, H.V.; Doriguetto, A.C.; et al. Nitrosyl/Diphenylphosphine/Amino Acid–Ruthenium Complexes as Inhibitors of MDA-MB-231 Breast Cancer Cells. *Inorganics* **2023**, *11*, 270. <https://doi.org/10.3390/inorganics11070270>

Academic Editors: Vladimir Arion, Dinorah Gambino, Célia S. Bonnet and Lubov Snegur

Received: 22 May 2023
Revised: 22 June 2023
Accepted: 23 June 2023
Published: 25 June 2023



Copyright: © 2023 by the authors. Licensee MDPI, Basel, Switzerland. This article is an open access article distributed under the terms and conditions of the Creative Commons Attribution (CC BY) license (<https://creativecommons.org/licenses/by/4.0/>).

1. Introduction

Metal-based complexes have been extensively studied as possible anticancer drugs, and since about fifty years ago, shown to be a very important class of chemotherapeutic agents. The most important anticancer metallodrug in cancer chemotherapy, cisplatin, was discovered in 1969 by Barnett Rosenberg and approved in the 1970s by the Food and Drug Administration (FDA) for the treatment of several solid tumors, including testicular, ovarian, bladder, and colorectal cancers [1–4]. Since then, many platinum complexes have been tested as anticancer drugs, and some of them have been approved, such as carboplatin and oxaliplatin [3]. Recently, since 2017, a palladium compound padeliporfin di-potassium, known by the trade name TOOKAD, has been authorized in Europe for use in vascular targeted photodynamic therapy (VTP) in the treatment of localized prostate cancer [5]. In general, the drugs commonly used in the clinic for the treatment of different type of cancers are accompanied by bothersome side effects; moreover, their effectiveness decreases with increasingly observed drug resistance. For these reasons, researchers around the world are actively searching for alternatives including new transition metal compounds, and ruthenium complexes have been proposed as possible new anticancer metallodrugs. Ruthenium complexes have been increasingly explored as potential anticancer agents, and it is observed that these compounds, in general, present octahedral geometry, which allows the allocation of different ligands in their coordination sphere. These characteristics

make ruthenium complexes a promising drug candidate, and in Figure 1, we present the structures of the ruthenium species that were or are in clinical trials [5]. However, despite the above, no ruthenium complex has been commercialized to date.

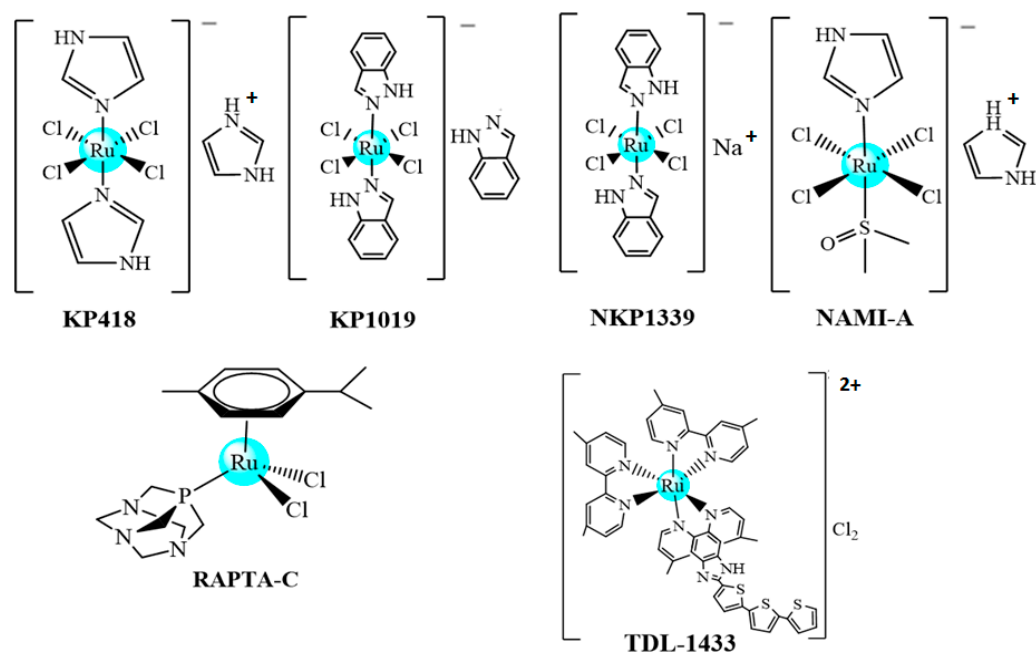


Figure 1. Ruthenium complexes that are or were in clinical tests.

In this context, ruthenium complexes have been intensively studied regarding the design of new transition metal compounds for biological applications [6–8]. It is known that the biological properties of this class of complexes can be improved through association with active ligands such as nitric oxide (NO), a molecule that plays an important role in the regulation of a wide range of physiological processes, including cytotoxic action, pertaining to tumor cells [9,10].

The metallic compounds can be modulated to act on potential molecular targets, and in the literature, there are some works describing ruthenium amino acid or NO complexes that have shown, in general, moderate activity *in vitro* against cancer cells [11–14].

The inclusion of diphosphines as ligands in the structure of ruthenium (II) complexes has given them great stability and good cytotoxicity against several cancer cells. In our previous work, cellular and molecular responses to treatment with Ru(II)/amino acid complexes, containing the 1,4-*bis*(diphenylphosphine)butane (dppb) ligand, in human triple-negative breast cancer cells showed their positive effects in multistep tumor metastasis. The complexes induced apoptosis by interfering with the DNA and mitochondria [14]. It should be mentioned that previously, we have explored the synthesis of some ruthenium complexes containing diphosphine ligands to evaluate their antitumor activity, and some of these complexes have shown promising results against different tumor cells [13,14]. Additionally, the nitrosyl complex [RuCl₂(NO)(BPA)] [BPA = (2-hydroxybenzyl)(2-methylpyridyl) amine ion] revealed significant activity against two different tumor cell lines (HeLa and Tm5), with efficacy comparable with cisplatin, and *in vivo* studies with this complex showed its capacity in reducing the tumor mass of tumor cells in mice [15]. Additionally, these nitrosyl ruthenium complexes presented high cytotoxic activities against the MDA-MB-231 human tumor cell line [15]. Notably, this kind of cancer is a very aggressive phenotype of breast cancer, with limited chemotherapeutic options [16].

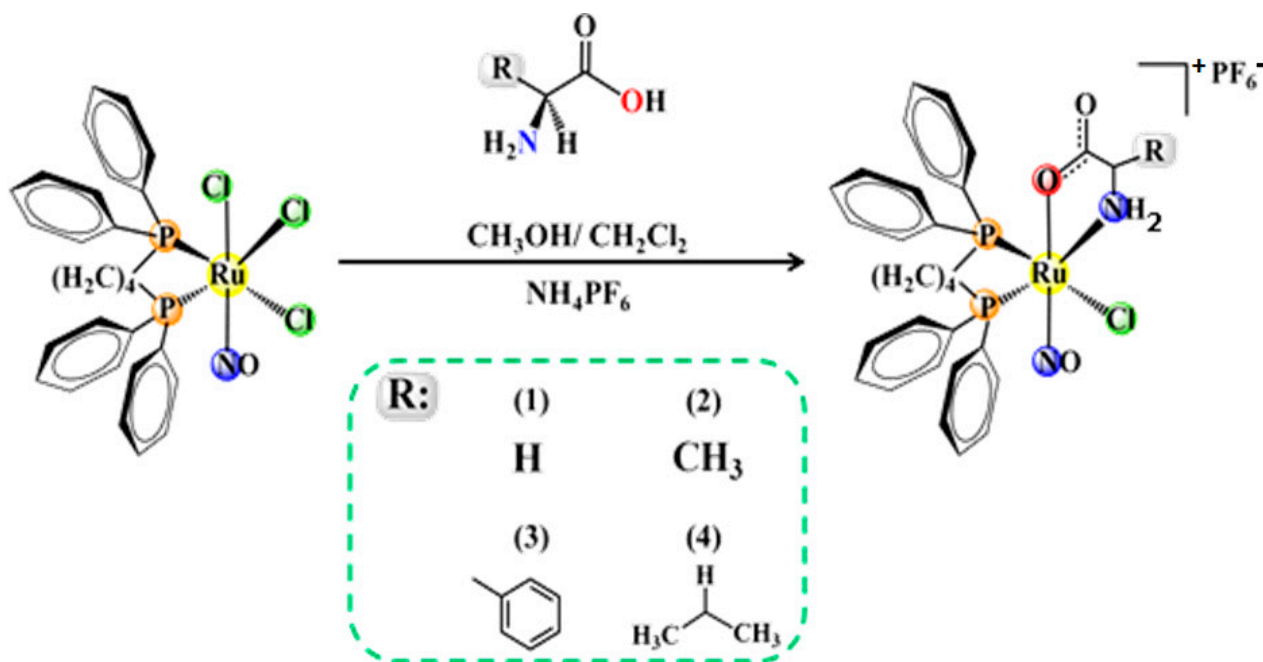
Furthermore, amino acid or nitrosyl and phosphine complexes have received attention because of their possible applications in biological and medicinal fields [17,18]. Therefore, as part of our continued interest in the development of new cytotoxic ruthenium(II)/diphosphine compounds, herein we report on complexes containing the bioactive

ligand nitric oxide, and amino acids; these were studied with the aim of evaluating the possible synergistic effect of the Ru/NO/AA-H system on the activity of the complexes. Thus, compounds with the general formula $[\text{RuCl}(\text{NO})(\text{AA-H})(\text{dppb})]\text{PF}_6$, (AA) = amino acids—glycine (1), L-alanine (2), L-phenylalanine (3), or L-valine (4) were synthesized, characterized, and tested against MDA-MB-231 cancer cells. The proposed formulations of the complexes were determined with a combination of techniques, such as NMR ($^{31}\text{P}\{^1\text{H}\}$, $^{13}\text{C}\{^1\text{H}\}$ and ^1H NMR), electronic absorption and infrared spectroscopies, elemental analyses, molar conductance, and X-ray diffraction for compounds (1) and (3).

2. Results and Discussion

2.1. Syntheses of the Compounds

The nitrosyl derivatives $[\text{RuCl}(\text{NO})(\text{AA-H})(\text{dppb})]\text{PF}_6$ [AA = glycine (1), L-alanine (2), L-phenylalanine (3), and L-valine (4)] were prepared from the *fac*- $[\text{RuCl}_3(\text{NO})(\text{dppb})]$ precursor [17]. As presented in the experimental section, the syntheses were carried out with good yields and with satisfactory elemental analysis data. The molar conductance measurements for the compounds are consistent with the 1:1 type, suggesting that after exchanging two chlorido ligands, the amino acid is coordinated in the O-N chelating mode, as a monoanionic ligand, *via* dissociation of the acid proton (Scheme 1).



Scheme 1. Synthesis of nitrosyl ruthenium (II) amino acid compounds.

2.2. Structural Studies

The crystal structures of complexes (1) and (3) were determined using single-crystal X-ray diffraction. Figure 1 shows the stereochemistry and the coordination sphere around the metal center, using an ORTEP representation. The crystallographic data show that complex (1) crystallizes in the monoclinic system with the space group $P2_1/n$, while complex (3) crystallizes in the non-centrosymmetric $P2_12_12_1$ orthorhombic group, as expected; this is because enantiopure L-amino acids were used as the starting material. In the two crystal structures, there is one molecule of complex, one PF_6^- , and one solvent molecule in the asymmetric unit (water in complex 1 and methanol in complex 3). Both complexes present the same stereochemistry, where the NO^+ ligand is *trans* to the oxygen atom from the amino acid, while the nitrogen atom is *trans* to one phosphorus atom from the dppb ligand. The other phosphorus atom from the dppb ligand is *trans* to a chlorido ligand (Figure 2).

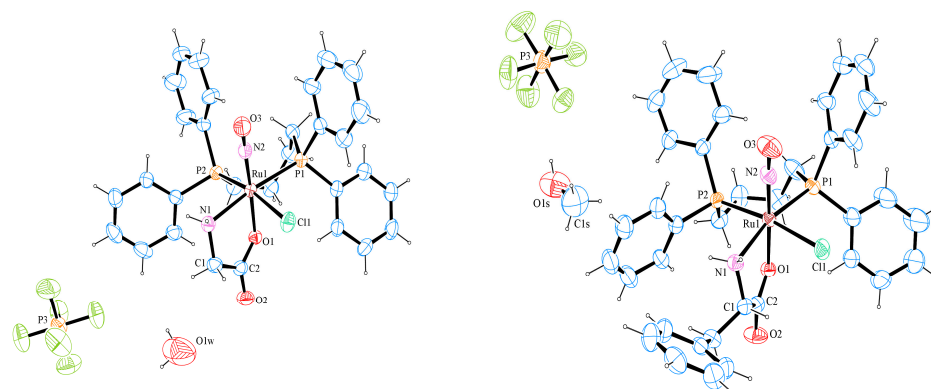


Figure 2. Crystal structures of $[\text{RuCl}(\text{NO})(\text{Gly-H})(\text{dppb})]\text{PF}_6 \cdot 0.5\text{H}_2\text{O}$ (**1**) (**left**) and $[\text{RuCl}(\text{NO})(\text{Phe-H})(\text{dppb})]\text{PF}_6 \cdot \text{CH}_3\text{OH}$ (**3**) (**right**), 30% probability ellipsoids for non-H atoms.

The main bond lengths and angles of (**1**) and (**3**) are shown in Table 1. The Ru–Cl, Ru–N, Ru–P, Ru–O, and N2–O3 bond lengths are similar when compared to the distances of other nitrosyl complexes previously reported in the literature [18–23]. The bond lengths of Ru1–Cl1 [2.4102(10) and 2.4121(9) Å], for complexes (**1**) and (**3**), respectively, with the chlorido ligand *trans* to phosphorus atoms, are slightly longer than those in which this ligand is positioned *trans* to the oxygen atom or *trans* to the nitrosyl ligand [19]. This is evidence of a structural *trans* effect of the phosphorus atoms.

Table 1. Selected bond and angle lengths (Å, °) for complexes (**1**) and (**3**).

Fragment	(1)	(3)
Ru(1)–N(2)	1.742(3)	1.727(3)
Ru(1)–O(1)	2.024(2)	2.003(2)
Ru(1)–N(1)	2.150(3)	2.164(2)
Ru(1)–P(1)	2.4027(10)	2.3968(8)
Ru(1)–P(2)	2.4004(10)	2.3975(9)
Ru(1)–Cl(1)	2.4102(10)	2.4121(9)
N(2)–O(3)	1.141(4)	1.148(4)
N(1)–C(2)	1.470(4)	1.489(4)
O(1)–C(1)	1.315(4)	1.315(4)
O(2)–C(1)	1.213(4)	1.215(4)
C(1)–C(2)	1.511(5)	1.521(5)
N(2)–Ru(1)–O(1)	174.23(12)	176.91(12)
N(2)–Ru(1)–N(1)	94.82(12)	98.09(12)
O(1)–Ru(1)–N(1)	80.20(10)	78.82(9)
N(2)–Ru(1)–P(1)	91.64(8)	91.39(10)
O(1)–Ru(1)–P(1)	81.08(7)	91.69(6)
N(1)–Ru(1)–P(1)	172.95(7)	167.31(7)
N(2)–Ru(1)–P(2)	89.16(10)	96.87(11)
O(1)–Ru(1)–P(2)	95.50(7)	83.22(7)
P(1)–Ru(1)–P(2)	93.21(4)	94.97(3)
N(2)–Ru(1)–Cl(1)	89.27(10)	89.81(11)
O(1)–Ru(1)–Cl(1)	87.37(7)	89.91(7)
N(1)–Ru(1)–Cl(1)	84.79(8)	83.10(9)
P(1)–Ru(1)–Cl(1)	89.45(4)	88.53(4)
P(2)–Ru(1)–Cl(1)	168.34(4)	172.37(3)
O(3)–N(2)–Ru(1)	172.2(3)	174.6(3)
C(1)–O(1)–Ru(1)	108.6(2)	119.1(2)

In the complexes with the general formula $(n\text{Bu}_4\text{N})[\text{RuCl}_3(\text{AA-H})(\text{NO})]$ (eight complexes), as characterized by X-ray diffraction, the coordinated oxygen from the carboxylate ion from the amino acid is also *trans* to the nitrosyl ligand, as detected in the complexes studied herein [22].

In the crystal structures of (1) and (3), it can be seen that the Ru1–N2–O3 bond angles are very close to 180° (Table 1), and their ruthenium centers present a slightly distorted octahedral geometry, as shown by the bond angles around the ruthenium ion. The N1–Ru–N2 and P1–Ru–N2 angles are close to the ideal value of 90°, whereas the chelate ring is very much distorted from the 90° angle, similar to the N1–Ru–O1 and P–Ru–P angle.

The crystal structure of the precursor, *fac*-[RuCl₃(NO)(dppb)], was previously reported, and the role of chloroform and acetone solvent on crystal self-assembly stabilization has been discussed [24]. In the same way, complexes (1) and (3) incorporate water and methanol, respectively, into their crystal lattice. The host solvent fits well in the cavity of the crystals.

2.3. ³¹P{¹H}, ¹³C{¹H} and ¹H NMR Studies

The ³¹P{¹H} NMR spectra of the new compounds present two doublets for compound (1), containing glycine, a non-chiral ligand, and four doublets for the compounds (2–4), suggesting the formation of diastereoisomers, as shown previously for other Ru(II)/amino acid complexes [18] (Figures S1–S4). The two phosphorus atoms of complexes (1–4) are magnetically nonequivalent, since P2 is *trans* to Cl[−] and P1 is *trans* to the nitrogen atom from the amino acid. The signal attributed to the phosphorous atom (P1) *trans* to the nitrogen of the amino acids is the most unshielded, while the most shielded signal refers to the phosphorous atoms (P2) *trans* to the Cl[−] ligand (σ- and π-donor). Due to the presence of diastereoisomers, the ¹H spectra of the complexes (2–4) (Figures S5–S8) are duplicated. In the ¹³C{¹H} NMR spectra of the complexes, the signals of C1 assigned to COO[−] (Figures 2 and 3), C2 to complex (1) and C3 for compounds (3) and (4) were shifted, indicating the coordination of amino acids via C1 of COO[−] and the nitrogen of NH₂, as observed in metal complexes with amino acid derivatives [18]. The chemical shifts of free ligands and complexes are summarized in Table 2. The duplicity of C1, C2, and C3 observed for compounds (1–4) is due to phosphorous–carbon coupling, and not to the presence of diastereoisomers as could be expected; it is in the order of ³J_{PC} 9.7 to 8.1 Hz, agreeing with the ³J_{PC} described in the literature [18] (Figures 3 and 4 for compounds (1) and (3), respectively, and Figures S9–S12). The phosphorous–carbon coupling is at the lowest distance observed for the C1 atom; as a consequence, the NO ligand, which presents a reverse *trans* effect, is *trans*-positioned to the O1 atom of the amino acid.

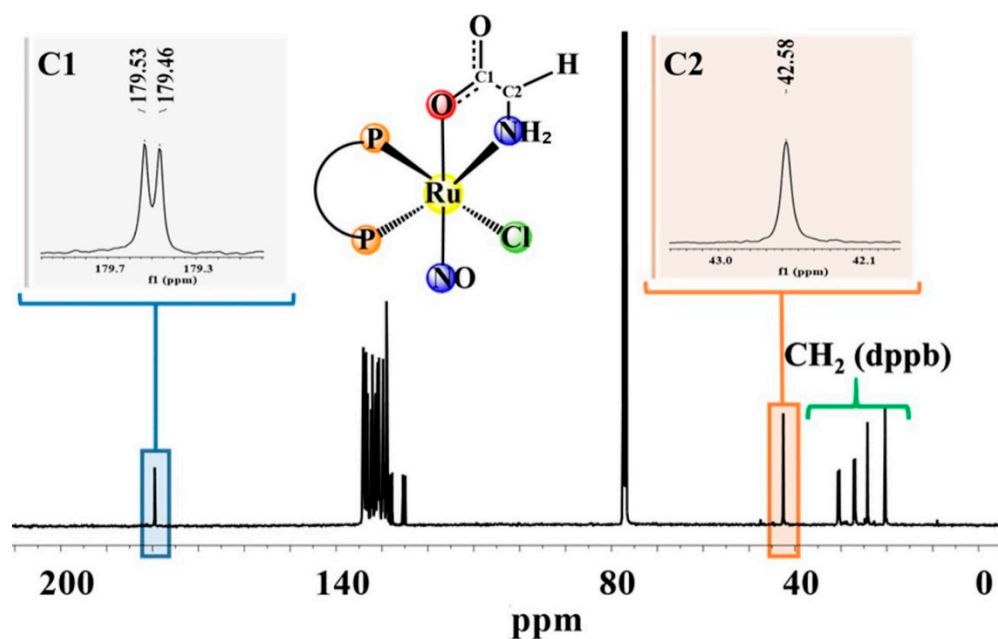
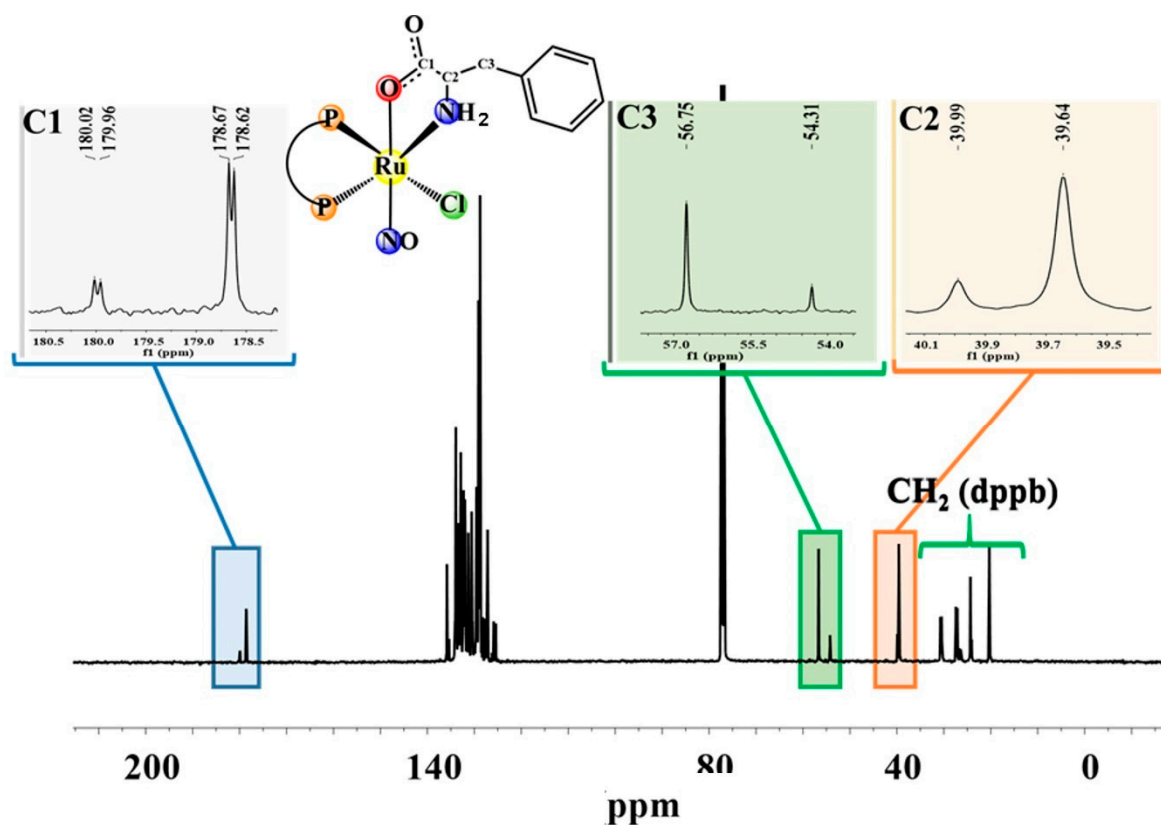


Figure 3. ¹³C{¹H} NMR spectrum for (1), in CDCl₃.

Table 2. $^{13}\text{C}\{^1\text{H}\}$ chemical shifts (ppm) for free amino acids and complexes (1–4).

$\delta^{13}\text{C}$ ppm (Free Amino Acids) (D_2O)				
	Gly	Ala	Phe	Val
C1	175.2 (s)	172.0 (s)	174.0 (s)	172.7 (s)
C2	43.2 (s)	51.4 (s)	56.9 (s)	59.6 (s)
C3	-----	33.0 (s)	37.2 (s)	30.0 (s)
$\delta^{13}\text{C}$ ppm (compounds) $[\text{RuCl}(\text{NO})(\text{AA-H})(\text{dppb})]\text{PF}_6$ (CDCl_3)				
	(1)	(2)	(3)	(4)
C1	179.4/179.3 (d) (9.7 Hz)	177.7/177.6 (d) (9.4 Hz) 176.6/176.3 (d) (9.0 Hz)	179.9/179.8 (d) (9.7 Hz) 178.6/178.5 (d) (8.1 Hz)	180.8/180.6 (d) (9.6 Hz) 179.8/179.6 (d) (8.1 Hz)
C2	43.0 (s)	52.3/50.1 (s)	56.9/54.0 (s)	60.6/53.4 (s)
C3	-----	37.0/35.0 (s)	39.0/35.0 (s)	30.5/29.3.0 (s)

**Figure 4.** $^{13}\text{C}\{^1\text{H}\}$ NMR spectrum for (3), in CDCl_3 .

The IR stretching frequencies of the $\nu(\text{NO})$ vibration are expected to be in the range $1800\text{--}1960\text{ cm}^{-1}$, and typical ranges for the values of internuclear N–O and M–N bond distances and M–N–O bond angles for linear nitrosyls are $1.14\text{--}1.20\text{ \AA}/1.60\text{--}1.90\text{ \AA}/180\text{--}160^\circ$. Thus, the structural parameters of the complexes (Tables 1 and 3) indicate that the nitrosyl ligand is linearly coordinated with the ruthenium center, and they are of the $[\text{RuNO}]^6$ type of nitrosyl ruthenium complex species [24–27] (Figures S13–S16). For all complexes, the IR spectra also confirm the presence of amino acid ligands coordinated with the metal. The bands assigned to the $\nu_s(\text{COO}^-)$ and $\nu_{as}(\text{COO}^-)$ for the free ligand and in the complexes are listed in Table 4. The value of $\Delta[\nu_{as}(\text{COO}^-)\nu_s(\text{COO}^-)]$, ranging from $310\text{ to }360\text{ cm}^{-1}$, shows that the ligand is coordinated to the metal in an N–O mode [18].

Table 3. Infrared frequencies (cm^{-1}) of the ligands and compounds *.

Free AA	ν_s (COO ⁻) (W)	ν_{ass} (COO ⁻) (S)	Complex	ν_s (COO ⁻) (W)	ν_{ass} (COO ⁻) (S)	ν (NO) (S)	$\Delta(\text{L})$	$\Delta(\text{C})$
Gly	1413	1592	(1)	1346	1683	1880	179	337
Ala	1417	1595	(2)	1379	1689	1876	183	310
Phe	1409	1584	(3)	1359	1690	1878	173	331
Val	1405	1591	(4)	1326	1686	1883	177	360

* Intensity stretch: (W) = weak/S = (strong)/ $\Delta(\text{L})$ = Ligands/ $\Delta(\text{C})$ = complexes.

Table 4. IC_{50} values and SI of complexes (1–4) against breast cancer (MDA-MB-231) cells and non-tumor (L929) cells.

Compound	IC_{50} (μM)		SI
	MDA-MB-231	L929	
(1)	33.6 ± 3.9	84.7 ± 3.1	2.5
(2)	25.9 ± 5.8	79.3 ± 2.5	3.1
(3)	12.1 ± 0.7	37.5 ± 4.7	3.1
(4)	23.9 ± 1.2	66.1 ± 4.2	2.8
Cisplatin	12.43 ± 0.20	29.0 ± 2.0	2.3

Data show means \pm SD of three independent experiments.

The UV-Vis electronic spectra of compounds (1–4), in CH_2Cl_2 , present bands with similar energies (c.a. 260 nm) and with high molar absorption coefficients (Figures S17–S20), which agree with the nitrosyl compounds described in the literature [15]. These bands at high energies are assigned to the intraligand transitions ($\pi \rightarrow \pi^*$) type. For these complexes, no bands of MLTC were observed due to the strong NO receptor character, which removes electron density from the metal center.

2.4. Biological Assays

2.4.1. Cytotoxicity of the Ru(II) Complexes

The MDA-MB-231 and L929 cells were exposed to the Ru(II) complexes (1–4) for 48 h to determine the cytotoxic activity of the compounds. The IC_{50} values for the complexes were calculated from the dose–survival values obtained using the MTT assay. As shown in Table 4, the complexes (1–4) are more sensitive to breast cancer cells than non-tumor cells. Despite the structural similarities of the complexes, complex (3) was the most active of the series, presenting the lowest value of IC_{50} and higher specificity for the cell MDA-MB-231, with SI values of 3.1. These results suggest that the phenyl group present in complex (3) can interact strongly with the DNA molecule, possibly through π – π interactions, making this complex more active than the others. Table 4 shows that complex (1) presented the highest value of IC_{50} and a lower SI.

The IC_{50} values found for complexes (1–4) are similar to those found for the complexes with general formula $[\text{Ru}(\text{AA-H})(\text{dppb})(\text{bipy})]\text{PF}_6$, described in the literature, containing the same diphosphine (dppb) ligands and the amino acids glycine, L-alanine, L-tyrosine, L-methionine, L-leucine, L-valine, L-serine, L-tryptophan, and L-lysine (AA-H). It is worth mentioning that for the complex $[\text{Ru}(\text{ser})(\text{dppb})(\text{bipy})]\text{PF}_6$, both isomers (Λ and Δ diastereoisomers) were isolated using HPLC experiments and the studies were performed with the isolated fractions, showing the same IC_{50} results for both fractions, within the experimental error and for all four cells tested [18]. Complexes with general formula $[\text{Ru}(\text{AA-H})(\text{P-P})(\text{N-N})]\text{PF}_6$ (where P-P = 1,4-bis(diphenylphosphine)butane (dppb) or 1,3-bis(diphenylphosphine)propane (dppp) and N-N = 4,4'-dimethyl-2,2'-bipyridine, 5,5'-dimethyl-2,2'-bipyridine or 4,4'-methoxy-2,2'-bipyridine, and AA-H are deprotonated L-amino acids) were tested against the MDA-MB-231 cancer cells, showing low IC_{50} values in the range 0.12–9.2 (μM) [28]. These Ru(II)/amino acid complexes showed good results

in vitro and in vivo. Therefore, variation of the amino acid ligand has a smaller impact on the cytotoxicity of the complexes within the range of amino acids employed, as observed by other researchers [29]. Thus, the cytotoxicity of Ru(II) complexes with the core “Ru(AA-H)(dppb)”, with or without the nitrosyl and containing diphosphine and amino acids (series [RuCl(NO)(AA-H)(dppb)PF₆ and [Ru(AA-H)(P-P)((N-N)]PF₆ as ligands, showed practically the same IC₅₀ for the MDA-MB-231 cancer cells [18,28]. Thus, with this in mind, work using photolysis on nitrosyl complexes is ongoing in our laboratory, aiming to release the NO group, which can produce reactive oxygen species (ROS). If successful, our nitrosyl complexes will be tested in the photodynamic therapy of cancer.

2.4.2. Ru(II) Complexes Induce Apoptosis in Cancer Cells

One of the strategies of antitumor drug design is to develop molecules that selectively induce the apoptosis of tumor cells. To evaluate the cell death mechanism induced by the complexes, morphological analysis was used, adopting HO/PI double-staining, and the typical morphological features of apoptosis and necrosis were considered. Cytological changes are classified according to the fluorescence emission and morphological features of cellular chromatin condensation in HO/PI-stained nuclei. Cells in apoptosis exhibit characteristic morphological changes, such as cellular shrinkage, chromatin condensation, DNA fragmentation, cytoplasmic blebbing, and cytoskeleton collapse (apoptotic bodies). Cells in early apoptosis (which still have intact membranes, but have begun undergoing DNA fragmentation) are stained blue, and cells in late apoptosis are stained purple (the blue and red color overlap) with condensed or fragmented chromatin. The necrotic cells swelled to large sizes, with uniform red fluorescent nuclei.

Figure 5 shows that all compounds decrease the percentage of viable cells and induce cell death by apoptosis in MDA-MB-231 cells. The percentages of apoptosis induced in MDA-MB-231 cells by complexes (1–4) were 47.0 ± 1.4%, 37.0 ± 2.8%, 32.5 ± 0.7%, and 25 ± 0.1%, respectively. For the untreated control, it was determined that 85.5 ± 0.7% were viable cells, 11.0 ± 1.4% were apoptotic cells, and 3.5 ± 0.7% of cells undergo necrosis.

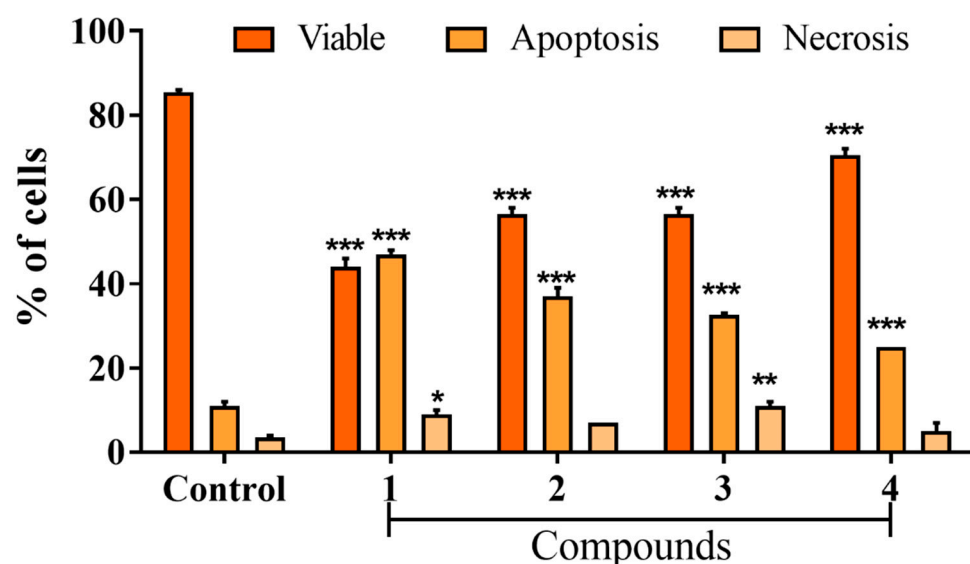


Figure 5. Effect on the mechanism of MDA-MB-231 cell death induced by Ru(II) complexes, evaluated by double-staining with Hoechst 33342 and propidium iodide. Percentage of apoptosis and necrosis in MDA-MB-231 cells 48 h post-treatment with Ru(II) complexes. Data show the means ± SD of two independent experiments. * $p < 0.05$, ** $p < 0.01$ and *** $p < 0.001$ indicate statistically significant differences from the untreated control.

The cell migration assay is one of the screening tools used to evaluate the antimetastatic properties of various compounds [29]. In addition, metastatic cancers have several important characteristics, including the migratory and invasive activities of tumor cells [30].

A wound healing assay was performed to verify the effect of the complexes on the motility of the MDA-MB-231 cells, after exposure of the complexes (1–4) to IC_{50} for 48 h. The complexes inhibited the migration capacity of MDA-MB-231 cells (Figure 6). The wound closure percentages of complexes (1–4) were $48.00 \pm 3.00\%$, $57.00 \pm 6.00\%$, $75.0 \pm 5.00\%$, and $70.00 \pm 5.00\%$, respectively, while for the untreated control, the percentage was $91.00 \pm 3.00\%$ (Figure 6). It is interesting to note that the cytotoxic activity of the complexes does not follow the same trend as the ability to inhibit cell migration ($1 > 2 > 4 > 3$), although all complexes demonstrated inhibition of cellular migration. Although complex (3) showed the best cytotoxicity result, it was not able to inhibit cell migration efficiently when compared to the others, indicating a cytotoxic complex with low anti-metastatic potential.

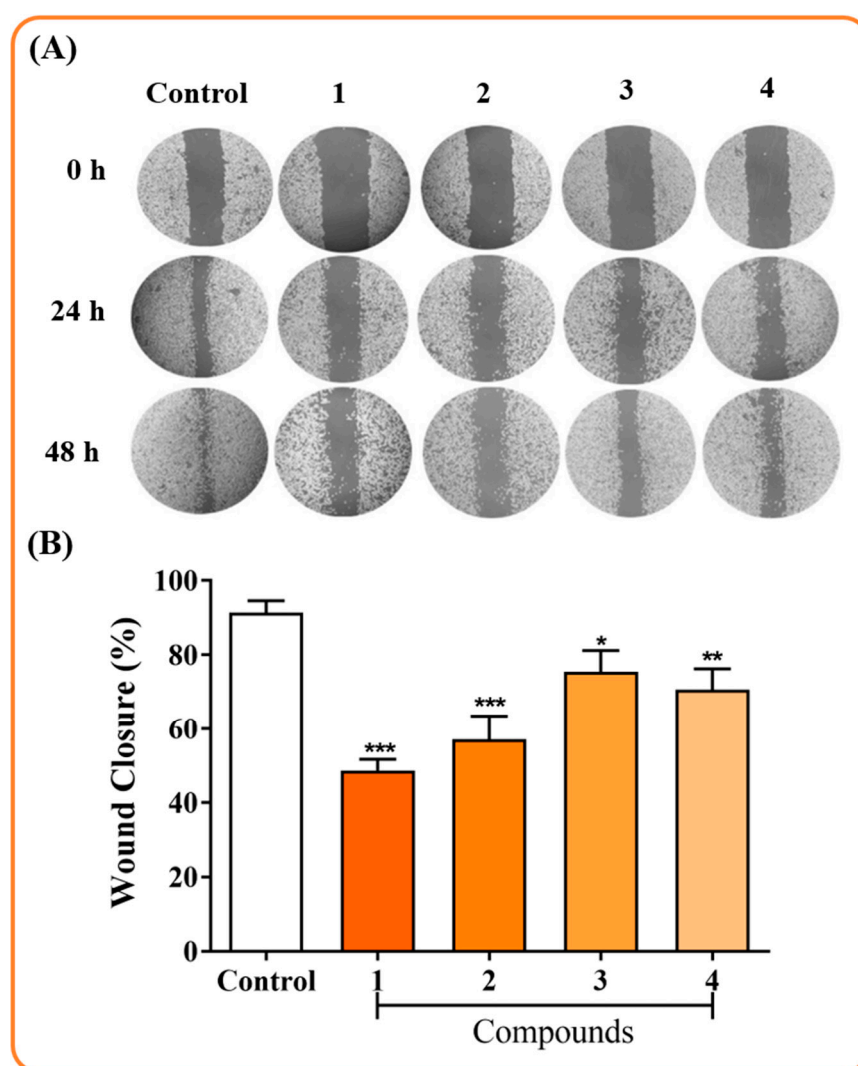


Figure 6. Effect on the migration inhibition of MDA-MB-231 cells after exposure to complexes (1–4) for 48 h. (A) Typical images of the wound at the beginning of the experiment up to 48 h post-treatment. (B) Wound closure in MDA-MB-231 cells after 48 h of incubation with Ru(II) complexes. Data show the means \pm SD of two independent experiments performed in triplicate. * $p < 0.05$, ** $p < 0.01$ and *** $p < 0.001$ indicate statistically significant differences from the untreated control.

HSA Fluorescence

HSA is the most abundant protein in blood plasma, associated with the transport and elimination of a wide variety of substances. With this in mind, the interaction of a complex with this protein is very important to understand [31]. The HSA exhibits fluorescence mainly due to tryptophan residue, and conformational changes due to the presence of

suppressors can affect this property, thus indicating interactions with the protein [32]. Therefore, in the investigation of the behavior of ruthenium/nitrosyl/amino acid compounds against HSA, a decrease was observed in the fluorescence intensity of the protein with an increase in the concentration of the complexes, as shown in Figure 7, for compound (1), indicating that the complexes interact with the HSA biomolecule [Figures S21–S23 for the compounds (2–4)].

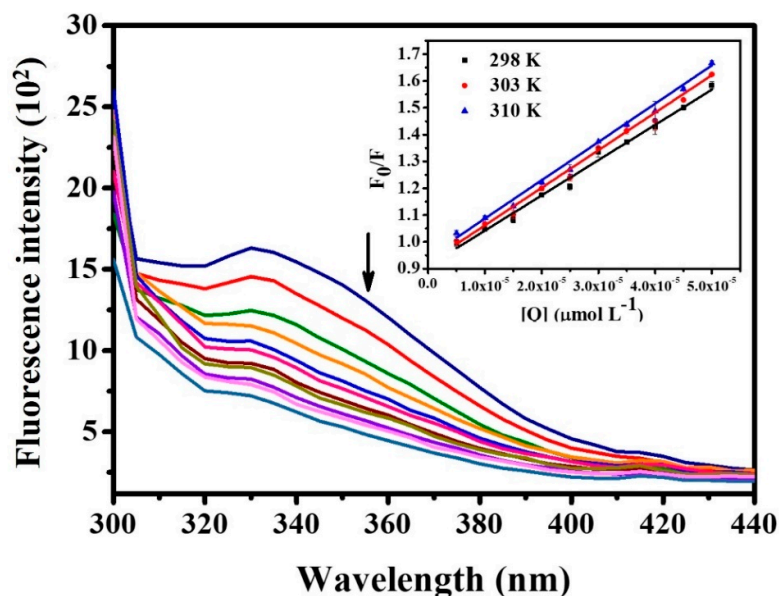


Figure 7. Fluorescence spectrum of HSA + $[\text{RuCl}(\text{NO})(\text{Gly-H})(\text{dppb})]\text{PF}_6$ (1). Concentration of HSA = $5.0 \mu\text{mol L}^{-1}$, $\lambda_{\text{ex.}} = 280 \text{ nm}$, $\text{pH} = 7.4$ e $T = 298 \text{ K}$. Inset: Stern–Volmer plots for the quenching of HSA fluorescence with $[\text{RuCl}(\text{NO})(\text{Gly-H})(\text{dppb})]\text{PF}_6$.

The values of K_{sv} , k_{q} , K_{b} , n and the thermodynamic parameters (ΔG° , ΔH° and ΔS°) are listed in Table 5, and for all complexes, the magnitude of the constant K_{sv} is in the order of 10^4 , which corroborates the literature data for ruthenium compounds, suggesting that the presence of the complexes does not cause major changes in the secondary structure of HSA [33,34]. We also observed that the K_{sv} values increase when the temperature is increased, which mainly indicates a dynamic suppression mechanism [35]. An explanation for the increase in the K_{sv} constant may be the greater diffusion of the suppressor when the experiment is performed at high temperatures, and consequently, the occurrence of a greater number of shocks between the suppressor and the HSA [35]. On the other hand, when comparing the bimolecular suppression speed constant, k_{q} , with the diffusional constant ($k_{\text{dif}} = 2 \times 10^{10} \text{ M}^{-1} \text{ s}^{-1}$), which limits the bimolecular process, a static type of mechanism is suggested. Thus, it is proposed that the two suppression mechanisms may occur in the system under study, and the predominance of one or the other may vary with the temperature [36].

The binding constants (K_{b}) vary between values in the order of 10^3 and 10^6 , suggesting interactions ranging from moderate to strong; the number of binding sites is approximately one. It is also observed that the K_{b} values decrease when the temperature increases, showing that the protein's capacity to store and transport this complex is impaired at higher temperatures [37]. Negative values for ΔG° indicate spontaneous HSA–complex interactions, and negative values of ΔH° and ΔS° indicate that the interactions of HSA–complex occur through van der Waals forces and hydrogen bonds [37]. The data obtained here are close to those shown for ruthenium complexes and previously described in the literature [11,38–40].

Table 5. Stern–Volmer quenching constant (K_{sv} , $L \text{ mol}^{-1}$), bimolecular quenching rate constant (k_q , $L \text{ mol}^{-1} \text{ s}^{-1}$), coefficient of determination of the Stern–Volmer relation (r^2), binding constant (K_b , mol L^{-1}), number of binding sites (n), ΔG (KJ mol^{-1}), and ΔH (KJ mol^{-1}) and ΔS ($\text{J mol}^{-1} \text{ K}^{-1}$) values for the complex–has system at the indicated temperature (K).

Complex	T (K)	$K_{sv} \cdot 10^4$	$k_q \cdot 10^{12}$	r^2	N	K_b	ΔG°	ΔH°	ΔS°
(1)	298	1.31 ± 0.04	2.62	0.993	1.37	$4.81 (\pm 0.29) \times 10^5$	−32.41	−89.85	−192.72
	303	1.40 ± 0.03	2.80	0.996	1.28	$1.94 (\pm 0.25) \times 10^5$	−30.67		
	310	1.43 ± 0.03	2.86	0.996	1.22	$1.18 (\pm 0.18) \times 10^5$	−30.10		
(2)	298	1.27 ± 0.04	2.54	0.991	1.50	$1.70 (\pm 0.29) \times 10^6$	−35.55	−65.12	−99.25
	303	1.37 ± 0.02	2.74	0.997	1.48	$0.75 (\pm 0.28) \times 10^6$	−34.07		
	310	1.36 ± 0.03	2.67	0.995	1.17	$0.62 (\pm 0.33) \times 10^6$	−34.35		
(3)	298	2.28 ± 0.08	4.56	0.990	0.89	$8.36 (\pm 0.20) \times 10^3$	−22.37	−77.25	−184.14
	303	2.34 ± 0.04	4.68	0.998	0.83	$4.56 (\pm 0.05) \times 10^3$	−21.22		
	310	2.31 ± 0.04	4.62	0.997	0.76	$2.50 (\pm 0.06) \times 10^3$	−20.87		
(4)	298	1.05 ± 0.03	2.10	0.994	1.13	$3.62 (\pm 0.13) \times 10^4$	−26.00	−41.05	−50.48
	303	1.14 ± 0.03	2.28	0.994	1.10	$3.16 (\pm 0.13) \times 10^4$	−26.10		
	310	1.24 ± 0.03	2.47	0.993	1.04	$1.90 (\pm 0.14) \times 10^4$	−25.40		

DNA Interaction Studies

DNA is one of the most studied biological targets when it comes to the development of metal-based chemotherapy, and its interaction with metallic compounds can be investigated using several techniques. Among these techniques, two were explored in this work: the relative viscosity of DNA, and a competitive assay with HOECHST 33258.

The viscosity experiments show the main types of interaction with DNA through the relationship between viscosity and the lengths of DNA fragments. Molecules that prolong the helix due to the separation of the base pair cause an increase in DNA viscosity, such as chloroquine and thiazole orange (Figure 8), which are intercalating molecules. When the complex can decrease the length of the DNA, it causes a decrease in the viscosity of the biomolecule. Cisplatin, for example, which covalently binds to the nitrogen bases of DNA, has this effect on this biomolecule. Weak interactions (electrostatic, groove interaction), and even non-interactions, do not cause significant changes in the viscosity profile of the DNA molecule [41–44].

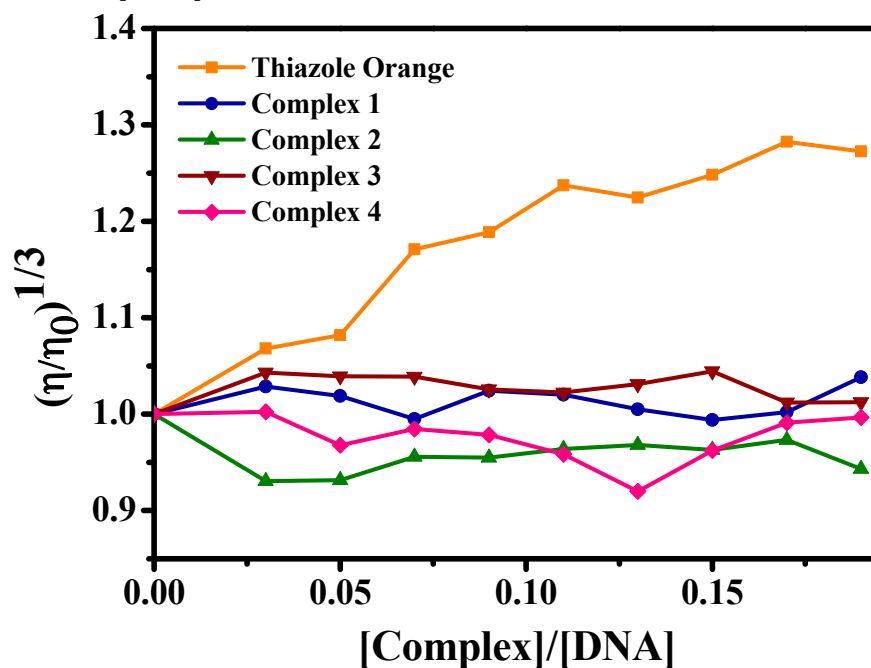


Figure 8. Effect of the concentration of complexes (1–4) and thiazole orange on the relative viscosity of CT-DNA at 25 °C.

Figure 8 shows that the compounds of ruthenium/nitrosyl/amino acids did not promote significant modifications in the CT-DNA viscosity profile, which excludes interactions via intercalation or covalence. Thus, to investigate the possible interaction complex/CT-DNA, a competitive experiment with HOECHST 33258 was used because it shows the possibility of the interaction of the complexes via minor CT-DNA grooves. HOECHST 33258 is a dye whose fluorescence increases considerably when it interacts with the CT-DNA molecule via minor grooves; it is used as a sensitive probe [45,46].

In Figure 9, the fluorescence spectra of the HOECHST-CT-DNA adduct are presented in the absence and presence of complexes in increasing concentrations, with a decrease in fluorescence intensity, especially for complex (3), in which this decrease is more significant. This suppression may indicate that the complexes interact with CT-DNA via minor grooves, or interact in such a way that it is possible to cause changes in this region via the biomolecule prompting the expulsion of HOECHST (and, therefore, a decrease in the fluorescence intensity). Similar results have already been observed for ruthenium/phosphine compounds, suggesting interaction via DNA grooves [33].

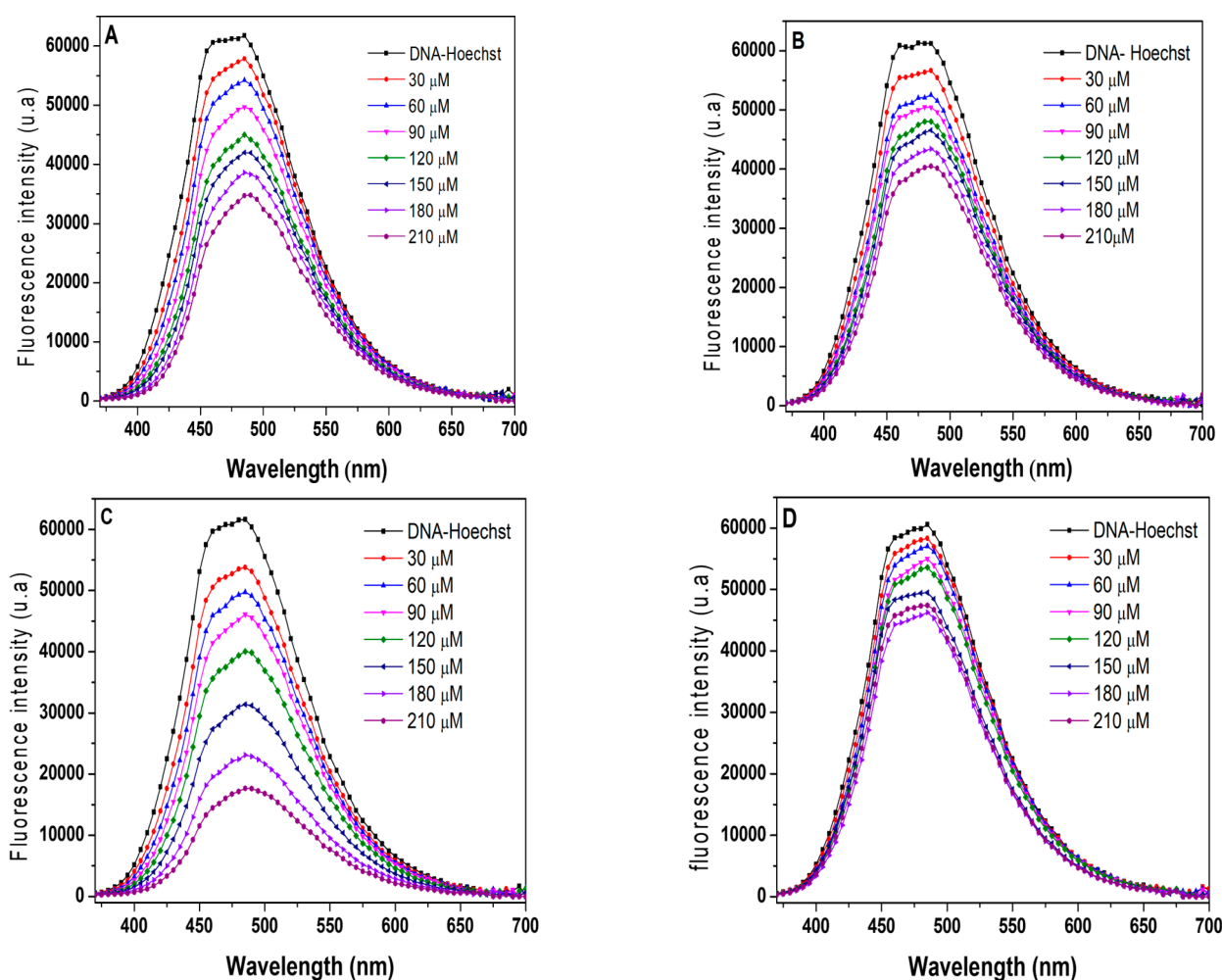


Figure 9. Emission spectra of the Hoechst adduct (5.3 μM)/CT-DNA (96.3 μM) in the presence of (A) complex 1, (B) complex 2, (C) complex 3, and (D) complex 4.

2.5. Study on the Stability of the Complexes

Time-dependent $^{31}\text{P}\{^1\text{H}\}$ NMR experiments in solution were carried out to evaluate the stability of the complexes in DMSO. Thus, complexes (1–4) were dissolved in DMSO and monitored using $^{31}\text{P}\{^1\text{H}\}$ NMR (using an external capillary with D_2O) (Figures 10 and S24–S26). The $^{31}\text{P}\{^1\text{H}\}$ NMR spectra reveal that complexes (1–4) are reason-

ably stable over a period of 48 h, but in some cases, a small amount of new and unknown product appears, mainly for complex (3).

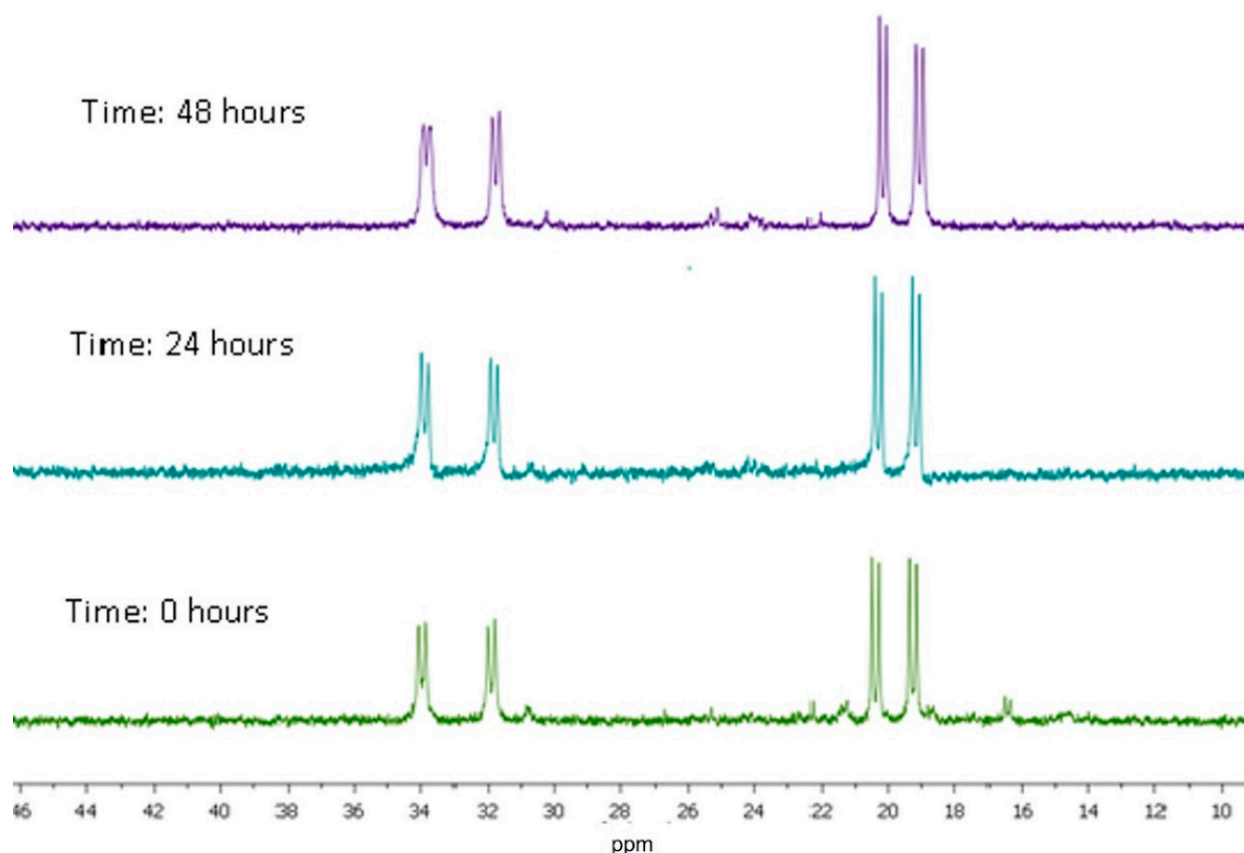


Figure 10. $^{31}\text{P}\{^1\text{H}\}$ NMR spectrum for complex (4) in DMSO-d_6 .

Thiols, such as glutathione (GSH), have been identified as activators of the nonenzymatic release of NO [44,45]. To reflect this situation, complexes (1) and (4) were incubated with a five-fold excess of GSH at 37°C in a mixture of $\text{DMSO}/\text{DMEM}/\text{GSH}$ solution [1M] (1:1:5), and monitored using $^{31}\text{P}\{^1\text{H}\}$ NMR (using an external capillary with D_2O) (see Supplementary Materials, Figures S27–S28). In the presence of GSH in the solution, after 48 h, sub-products were observed. Interestingly, the signal observed at δ 42.0 ppm could be indicative of the reduction of the NO^+ group, by the glutathione, forming complexes without the nitrosyl ligand, which is dissociated from the ruthenium(II) center. This suggestion finds support in the literature, in which it is shown that the glutathione (or cysteine) can reduce the coordinated Ru-NO^+ , which is dissociated from the original complex, thereby forming products with a coordinating solvent [47,48]. In our case, considering that in the DMEM solution there are different aminoacids, products with different formulations can be formed, including $[\text{Ru}(\text{dppb})(\text{AA-H})_2]$, for instance, which can show a chemical shift of up to 40 ppm. In this case, both nitrogen atoms from the amino acids are *cis* to each other, and *trans* to the phosphorus atoms from the dppb ligand.

3. Experimental Section

3.1. Materials for Synthesis

Solvents were purified using standard methods. All chemicals used were of reagent grade or comparable purity. The $\text{RuCl}_3 \cdot 3\text{H}_2\text{O}$ and the ligands 1,4-bis(diphenylphosphino)butane (dppb) and amino acids (glycine, L-alanine, L-phenylalanine, and L-valine) were used as received from Sigma-Aldrich, St. Louis, MO, USA. Calf thymus DNA (CT-DNA) from SIGMA type I N $^\circ$ D-1501 was used for corresponding DNA studies. The HSA was also received from Sigma-Aldrich. The precursor, *fac*- $[\text{RuCl}_3(\text{NO})(\text{dppb})]$, was prepared

following the protocol described in the literature [17]. NO_(g) was generated via the reaction of metallic copper and a solution of HNO₃ (33% concentration).

3.2. Instrumentation

Elemental analyses were performed in a Fisons EA 1108 model (Thermo Scientific, Waltham, MA, USA). The FTIR spectra of the powder complexes were recorded using KBr pellets in the 4000–200 cm⁻¹ region, in an FT MB-102 instrument (Bomen–Michelson, St. Jean-Baptiste, Quebec, Canada). The UV-Vis spectra of the complexes were recorded in CH₂Cl₂ solution, in a Hewlett Packard diode array, 8452A. All the NMR spectra were recorded at 298 K and measured using a 9.4 T Bruker Avance III spectrometer (Berlin, Germany), observing ¹H at 400.13 MHz, ¹³C NMR (100.52 MHz), and ³¹P{¹H} at 161.98 MHz. The NMR spectra were recorded in CDCl₃(complexes) or D₂O (amino acids), with TMS (¹H and ¹³C) as reference. The ³¹P{¹H} NMR spectra were recorded in CH₂Cl₂ using a capillary containing D₂O, with H₃PO₄ 85% as a reference. The molar conductivity measurements (Λ_m) were taken in acetone at 298 K, using concentrations of 1.0 × 10⁻³ M for the complexes.

3.3. X-ray Crystallography

Yellow crystals of [RuCl(NO)(Gly-H)(dppb)]PF₆·0.5H₂O (1) and [RuCl(NO)(Phe-H)(dppb)]PF₆·CH₃OH (3) were obtained via slow evaporation of a dichloromethane/methanol solution (1:2) with a drop of water, at 298 K. Attempts were made to obtain crystals of compounds (2) and (4) using the same methodology, but unfortunately the crystals obtained were amorphous and unsuitable for determining their structures using X-rays. The data collection was performed using Mo-Kα radiation (λ = 0.71073 Å) on an Enraf–Nonius Kappa-CCD diffractometer at 293 K. Data reduction was carried out using Denzo-SMN and Scalepack software [49]. The structures were solved with a direct method using SHELXS-97, and refined using the software SHELXL-97 [50]. The hydrogen atoms were calculated at idealized positions using the riding model option of SHELXL97 [50]. The Gaussian method was used for the absorption corrections [51]. ORTEP-3 [52] was used to generate the molecular graphics. Table 6 summarizes the main crystallographic data for complexes (1) and (3).

Table 6. Crystal data and structure refinement for [RuCl(NO)(Gly-H)(dppb)]PF₆·0.5 H₂O (1) and [RuCl(NO)(Phe-H)(dppb)]PF₆·CH₃OH (3) complexes.

	(1)	(3)
Empirical formula	C ₃₀ H ₃₂ ClF ₆ N ₂ O ₃ P ₃ Ru·0.5 H ₂ O	C ₃₇ H ₃₈ ClF ₆ N ₂ O ₃ P ₃ Ru·CH ₃ OH
Molecular weight	821.01	934.17
Temperature (K)	293(2) K	293(2) K
Wavelength (MoKα) (Å)	0.71073 Å	0.71073 Å
Crystal system	Monoclinic	Orthorhombic
Space group	P2 ₁ /n	P2 ₁ 2 ₁ 2 ₁
Unit cell dimensions (Å; °)	a = 11.0010(4) Å b = 10.8570(5) Å; β = 98.649(4)° c = 28.8450(15) Å	a = 9.26250(10) Å b = 14.6732(3) Å c = 30.1005(6) Å
Volume	3406.0(3) Å ³	4090.97(12) Å ³
Z	4	4
Density (calculated; Mg/m ³)	1.601 Mg/m ³	1.517 Mg/m ³
Absorption coefficient (mm ⁻¹)	0.749 mm ⁻¹	0.635 mm ⁻¹
F(000)	1660	1904
Crystal size (mm ³)	0.06 × 0.14 × 0.22 mm ³	0.11 × 0.18 × 0.31 mm ³
Theta range for data collection (°)	3.05 to 26.73°	2.93 to 26.74°
Index ranges	−11 ≤ h ≤ 13, −12 ≤ k ≤ 13, −35 ≤ l ≤ 36	−8 ≤ h ≤ 11, −18 ≤ k ≤ 18, −38 ≤ l ≤ 38
Reflections collected	17,276	24,378
Independent reflections	7182 [R(int) = 0.0571]	8659 [R(int) = 0.0280]
GoF	1.072	1.095

Table 6. Cont.

	(1)	(3)
Max. and min. transmission	0.948 and 0.876	0.936 and 0.852
R1; wR2 [I > 2σ (I)]	0.0453; 0.0963	0.0395; 0.0876
R1; wR2 (Total)	0.0841; 0.1063	0.0416; 0.0889
Largest diff. peak and hole	0.478 and $-0.625 \text{ e} \cdot \text{Å}^{-3}$	0.500 and $-0.352 \text{ e} \cdot \text{Å}^{-3}$

GoF = Goodness of fit; R1 = agreement between the calculated and observed models based on the structure factors (F); wR2 = agreement between the calculated and observed models based on the square of the structure factors (F²).

3.4. Synthesis of Complexes 1–4

[RuCl(NO)(Gly-H)(dppb)]PF₆·H₂O (1): Briefly, 11.26 mg (0.15 mmol) of the amino acid glycine was dissolved in a Schlenk flask in 20 mL of deoxygenated methanol, and kept under reflux until complete solubilization. Next, 100 mg (0.15 mmol) of the precursor *fac*-[RuCl₃(NO)(dppb)], dissolved in 10 mL of dichloromethane, was added to the flask. This mixture was kept under argon atmosphere, stirring and reflux for 1 h, and 24.45 mg (0.15 mmol) of NH₄PF₆ was added. The solution was maintained in this condition for 24 h. After this time, the volume of the solution was reduced to about 1 mL, and the addition of degassed diethyl ether resulted in the precipitation of a yellow solid. The solid was filtered off, washed with water and diethyl ether, and dried in a vacuum. Yield: 0.10 g; 84.3%. Anal. Calc. for C₃₀H₃₄ClF₆N₂O₄P₃Ru: exp. (calc) C 43.6 (43.4), H 4.0 (4.1), N 3.7 (3.4). Molar conductance (μS/cm, CH₂Cl₂) 81.4. IR (cm⁻¹): 3313, 3056, 2942, 1875, 1661, 1592, 1413, 1258, 1305, 1095, 849, 751, 697, 552, 498, 335. UV-Vis [CH₂Cl₂, λ/nm (ε/M⁻¹ cm⁻¹)]: 260 (1.52 × 10³). ³¹P{¹H} NMR (161.98 MHz, in CH₂Cl₂/D₂O at 298K): 33.8 ppm (d) and 20.8 ppm (d) MHz (²J_{P-P} = 26.2 Hz). ¹H NMR (400.21 MHz, CDCl₃): δ(ppm) 7.4–8.1 overlapped signals (20H atoms of aromatic hydrogens of dppb), 2.9–1.4 (8H, CH₂ of dppb), 2.1 (s) (2H of CH₂ of Gly), 1.3 (s) (1H of NH of Gly). ¹³C{¹H} NMR (400.21 MHz, CDCl₃): δ(ppm) (CH₂ of dppb): 20.9 (s, CH₂), 24.1 (s, CH₂), 26.5 (d, CH₂), 30.3 (d, CH₂), (CH₂ of Gly): 42.4 (s), (C of dppb): 127.6–134.0, (C = O of Gly) 179.3 (d, ¹J_{C-P} = 9.7 Hz).

[RuCl(NO)(Ala-H)(dppb)]PF₆ (2): In a Schlenk flask, 13.37 mg (0.15 mmol) of L-alanine was dissolved in 20 mL of deoxygenated methanol and refluxed until complete solubilization, after which 100.0 mg (0.15 mmol) of the precursor *fac*-[RuCl₃(NO)(dppb)], dissolved in 10 mL of dichloromethane, was added to the flask. This mixture, under argon atmosphere and stirring, was refluxed for 1 h, and 24.45 mg (0.15 mmol) of NH₄PF₆ were added. The solution was maintained in this condition for 24 h, and after this time, the volume of the solution was reduced to about 1 mL. The addition of degassed diethyl ether resulted in the precipitation of a yellow solid, which was filtered off, washed with water and diethyl ether, and dried in a vacuum. Yield: 0.11 g; 86.5%. Anal. Calc. for C₃₁H₃₃ClF₆N₂O₃P₃Ru: exp. (calc) C 44.7 (45.1), H 4.2 (4.0), N 3.3 (3.4). Molar conductance (μS/cm, CH₂Cl₂) 62.9. IR (cm⁻¹): 3333, 3262, 3058, 2908, 1884, 1687, 1435, 1085, 988, 846, 755, 694, 552, 501. UV-Vis [CH₂Cl₂, λ/nm (ε/M⁻¹ cm⁻¹)]: 265 (3.44 × 10³). ³¹P{¹H} NMR (161.98 MHz, in CH₂Cl₂/D₂O at 298K): 34.1 ppm (d) and 20.4 ppm (d) MHz (²J_{P-P} = 26.8 Hz) and 32.1 ppm (d) and 19.2 ppm (d) MHz (²J_{P-P} = 26.4 Hz). ¹H NMR (400.21 MHz, CDCl₃): δ(ppm) 7.3–8.0 overlapped signals (20H atoms of aromatic hydrogens of dppb), 4.0 (1H of CH of Ala), 3.5–1.6 (8H, CH₂ of dppb), 1.6 (s) (1H of NH of Ala), 1.0 (s) (3H of CH₃ of Ala). ¹³C{¹H} NMR (400.21 MHz, CDCl₃): δ(ppm) (CH₂ of dppb): 21.3 (s, CH₂), 24.8 (s, CH₂), 26.7 (d, CH₂), 31.3 (d, CH₂), (CH₃ of Ala): 37.0 and 35.0, (CH of Ala): 52.3 and 50.1, (C of dppb): 125.1–138.0, (C = O of Ala) 176.5 (d, ¹J_{C-P} = 9.0 Hz) and 177.6 (d, ¹J_{C-P} = 9.4 Hz).

[RuCl(NO)(Phe-H)(dppb)]PF₆·CH₃OH (3): Briefly, 24.78 mg (0.15 mmol) of L-phenylalanine was dissolved in a Schlenk flask in 20 mL of deoxygenated methanol and kept under reflux until complete solubilization. After, 100.0 mg (0.15 mmol) of the precursor *fac*-[RuCl₃(NO)(dppb)], dissolved in 10 mL of dichloromethane, was added to the flask. This mixture was kept under argon atmosphere, stirring and reflux for 1 h, and 24.45 mg

(0.15 mmol) of NH_4PF_6 was added. The solution was maintained in this condition for 24 h, and after this time, the volume of the solution was reduced to about 1 mL; the addition of degassed diethyl ether resulted in the precipitation of a yellow solid, which was filtered off, washed with water and diethyl ether, and dried in a vacuum. Yield: 0.10 g; 67.0%. Anal. Calc. for $\text{C}_{38}\text{H}_{41}\text{ClF}_6\text{N}_2\text{O}_4\text{P}_3\text{Ru}$: exp. (calc) C 49.0 (48.9), H 4.1 (4.4), N 3.2 (3.0). Molar conductance ($\mu\text{S}/\text{cm}$, CH_2Cl_2) 68.9. IR (cm^{-1}): 3284, 3055, 2923, 1875, 1682, 1450, 1418, 1286, 1198, 1092, 986, 898, 845, 744, 684, 553, 502. UV-Vis [CH_2Cl_2 , λ/nm ($\epsilon/\text{M}^{-1}\text{cm}^{-1}$): 267(3.44×10^3). $^{31}\text{P}\{^1\text{H}\}$ NMR (161.98 MHz, in $\text{CH}_2\text{Cl}_2/\text{D}_2\text{O}$ at 298K): 35.5 ppm (d) and 20.4 ppm (d) MHz ($^2J_{\text{P-P}} = 25.8$ Hz) and 27.9 ppm (d) and 22.0 ppm (d) MHz ($^2J_{\text{P-P}} = 24.9$ Hz). ^1H NMR (400.21 MHz, CDCl_3): δ (ppm) 6.7–8.1 overlapped signals (25H atoms of aromatic hydrogens of dppb and Phe), 4.0 (1H of CH of Phe), 3.5–3.0 (2H, CH_2 of Phe), 3.0–1.6 (8H, CH_2 of dppb), 1.7 (s) (1H of NH of Phe). $^{13}\text{C}\{^1\text{H}\}$ NMR (400.21 MHz, CDCl_3): δ (ppm) (CH_2 of dppb): 20.3 (s, CH_2), 24.4 (s, CH_2), 27.3 (d, CH_2), 30.6 (d, CH_2), (CH_2 of Phe): 39.0 and 35.0, (CH of Phe): 56.9 and 54.0, (C of dppb): 126.0–137.0, (C = O of Phe) 189.8 (d, $^1J_{\text{C-P}} = 9.7$ Hz) and 177.6 (d, $^1J_{\text{C-P}} = 8.1$ Hz).

[$\text{RuCl}(\text{NO})(\text{Val-H})(\text{dppb})$] PF_6 (4): Briefly, 17.58 mg (0.15 mmol) of L-valine was dissolved in a Schlenk flask in 20 mL of deoxygenated methanol, and kept under reflux until complete solubilization. Afterwards, 100.0 mg (0.15 mmol) of the precursor *fac*-[$\text{RuCl}_3(\text{NO})(\text{dppb})$], dissolved in 10 mL of dichloromethane, was added to the flask, and this mixture, under argon atmosphere, was stirred and refluxed for 1 h, after which 24.45 mg (0.15 mmol) of NH_4PF_6 was added. The solution was maintained in this condition for 24 h, and after this time, the volume of the solution was reduced to about 1 mL; the addition of degassed diethyl ether resulted in the precipitation of a yellow solid, which was filtered off, washed with water and diethyl ether, and dried in a vacuum. Yield: 0.10 g; 79%. Anal. Calc. for $\text{C}_{33}\text{H}_{38}\text{ClF}_6\text{N}_2\text{O}_3\text{P}_3\text{Ru}$: exp. (calc) C 46.0 (46.4), H 4.0 (4.5), N 3.1 (3.3). Molar conductance ($\mu\text{S}/\text{cm}$, CH_2Cl_2) 88.1. IR (cm^{-1}): 3249, 3053, 2920, 1870, 1684, 1434, 1301, 1088, 999, 845, 754, 703, 560, 509. UV-Vis [CH_2Cl_2 , λ/nm ($\epsilon/\text{M}^{-1}\text{cm}^{-1}$): 270 (4.28×10^3). $^{31}\text{P}\{^1\text{H}\}$ NMR (161.98 MHz, in $\text{CH}_2\text{Cl}_2/\text{D}_2\text{O}$ at 298K): 33.5 ppm (d) and 18.7 ppm (d) MHz ($^2J_{\text{P-P}} = 23.1$ Hz) and 31.0 ppm (d) and 20.0 ppm (d) MHz ($^2J_{\text{P-P}} = 21.2$ Hz). ^1H NMR (400.21 MHz, CDCl_3): δ (ppm) 7.2–8.3 overlapped signals (20H atoms of aromatic hydrogens of dppb), 4.0 (1H of CH of Val), 3.2 (1H of CH of Val), 3.5–2.5 (8H, CH_2 of dppb), 3.2 (s) (6H of CH_3 of Val), 1.8 (s) (1H of NH of Val). $^{13}\text{C}\{^1\text{H}\}$ NMR (400.21 MHz, CDCl_3): δ (ppm) (CH_2 of dppb): 19.1 (s, CH_2), 23.1 (s, CH_2), 26.9 (d, CH_2), 30.1 (d, CH_2), (CH_2 of Val): 30.5 and 29.3, (CH of Val): 60.6 and 53.4, (C of dppb): 126.0–138.0, (C = O of Val) 180.7 (d, $^1J_{\text{C-P}} = 9.6$ Hz) and 179.7 (d, $^1J_{\text{C-P}} = 8.1$ Hz).

3.5. Cell Culture

The MDA-MB-231 (triple-negative breast cancer) and L929 cells (non-tumor murine fibroblast) were routinely cultured in DMEM medium (Sigma-Aldrich, St. Louis, MO, USA) supplemented with 10% fetal calf serum, L-glutamine, and penicillin/streptomycin. Cell cultures were maintained in a humidified incubator (Thermos Scientific, Marietta, OH, USA) at 37 °C with 5% CO_2 .

3.5.1. MTT Assay

The MDA-MB-231 (1.5×10^4 cells per well) and L929 (1.0×10^4 cells per well) cells were seeded in a 96-well tissue culture plate for 24 h. Afterward, the cells were incubated with different concentrations (0.2–200 μM) of the Ru(II) complexes for 48 h. Then, cell viability was measured by the ability of cells to transform MTT into a purple formazan dye, which was carried out as described previously [53]. MTT solution (1 mg mL^{-1}) was added to each well plate, and plates were incubated for 3 h at 37 °C. Finally, the purple formazan crystals were dissolved by adding 10% SDS/0.01N HCl solution. The absorbance was determined at 545 nm using a Stat Fax 2100 microplate reader (Awareness Technology, Palm City, FL, USA). The IC_{50} (concentration required for 50% inhibition of cell viability) values were obtained via nonlinear regression using GraphPad Prism 5.01 for Windows. The

cytotoxicity was assessed in terms of the selectivity index (SI) for each Ru(II) complex, with the following: $SI = IC_{50}(\text{non-tumor cells})/IC_{50}(\text{tumor cells})$. Cytotoxicity was considered significant when $SI \geq 2.0$.

All experiments were carried out in triplicate and independently to assure the reliability of results. Data were expressed as means \pm S.D. Determination of IC_{50} , statistical measurements, and graphics were carried out in GraphPad Prism software (Intuitive Software for Science, San Diego, CA). The results were compared using a one-way ANOVA (acceptable significance $p < 0.05$), followed by Dunnett's test, which compares all groups with control group.

The complexes (1–4) are not soluble in water, but are soluble in dichloromethane, methanol, and dimethylsulphoxide. In this case, for the biological experiments, solutions of 10% DMSO and 90% DMEM (*v/v*) were used.

3.5.2. Assessment of Apoptosis and Necrosis

Briefly, 2×10^5 of MDA-MB-231 cells were treated at IC_{50} with each compound for 48 h. Afterward, the cells were scratched and washed with PBS. The cells were suspended in Hoechst 33342 solution ($10 \mu\text{g mL}^{-1}$) and propidium iodide ($2.5 \mu\text{g mL}^{-1}$), and incubated at 37°C for 10 min in total darkness. The slides were analyzed using a fluorescence microscope (Leica, Wetzlar, Germany). At least 300 target cells were counted on each slide, and each experiment was performed in duplicate. The percentages of apoptotic (early and late apoptosis) and necrotic cells were determined from the total number of cells: (a) viable—blue chromatin with an organized structure, (b) early apoptosis—bright blue chromatin that is highly condensed or fragmented, (c) late apoptosis—bright pink chromatin that is highly condensed or fragmented, and (d) necrosis—pink chromatin with an organized structure [54–56].

3.5.3. Wound Healing Assay

To verify whether Ru(II) complexes can block the migration of cell metastasis, a wound healing assay was performed. The MDA-MB-231 (2×10^5 cells per well) cells were seeded in a 6-well tissue culture plate for 24 h. Scratch wounds were made in the monolayer using a tip (200 μL). The medium was replaced, and then the MDA-MB-231 cells were treated at IC_{50} with each compound for 48 h. Migration cells were imaged every 24 h for 2 days. The images were analyzed using Image J software (Rasband, W.S., ImageJ, U. S. National Institutes of Health, Bethesda, Maryland, USA) to quantify the distance and to determine the wound closure ratio.

3.6. HSA Fluorescence

The interaction of the complexes with HSA was measured by carrying out the suppression of fluorescence in a microplate reader, model SpectraMax M3. A $5.0 \mu\text{mol L}^{-1}$ protein solution in Tris-HCl pH 7.4 buffer was thusly prepared. The concentration of HSA was determined spectrophotometrically, through absorbance analysis, using a molar extinction coefficient of $35,700 \text{ M}^{-1} \text{ cm}^{-1}$ at 280 nm [57]. Protein interactions were examined in 96-well plates used for fluorescence assays. The excitation wavelength was 280 nm, and the emission was recorded in the range of 300 to 500 nm. Compound solutions were prepared in DMSO and incubated with HSA at different molar ratios. The extinction of the emission intensity was monitored at different temperatures (298, 303 and 310 K). The experiments were carried out in triplicate and analyzed using the Stern–Volmer equation:

$$F_0/F = 1 + K_q\tau_0[Q] = 1 + K_{sv}[Q] \quad (1)$$

where F_0 and F are the fluorescence intensities in the absence and presence of quenchers, respectively, $[Q]$ is the quencher concentration, and K_{sv} is the Stern–Volmer quenching constant, which can be written as $K_q = K_{sv}/\tau_0$, where K_q is the bimolecular quenching rate constant and τ_0 is the average lifetime of the fluorophore in the absence of quencher

(5.9×10^{-9} s). Therefore, Equation (1) was applied to determine Ksv, using linear regression of a plot of F_0/F vs. $[Q]$.

The binding constant (K_b) and the number of binding sites were determined by plotting the double-logarithmic graph of the fluorescence data using Equation (2), as well as the thermodynamic parameters of Equations (3) and (4). K_1 and K_2 are the binding constants at temperatures T_1 and T_2 , respectively, and R is the gas constant.

$$\log \frac{(F_0 - F)}{F} = \log K_b + n \log [Q] \quad (2)$$

$$\ln \left(\frac{K_{b1}}{K_{b2}} \right) = \left(\frac{1}{T_1} - \frac{1}{T_2} \right) \times \frac{\Delta H^\circ}{R} \quad (3)$$

$$\Delta G^\circ = -RT \ln K_b = \Delta H^\circ - T \Delta S^\circ \quad (4)$$

3.7. Interaction with DNA

3.7.1. Viscosity

The relative viscosity of the DNA was measured using an Ostwald viscometer, maintained at a constant temperature of 298 K in a thermostatic bath. The CT-DNA solution in Tris-HCl buffer (5.0 mM Tris-HCl, 50 mM NaCl, pH = 7.4) was fixed at 140 μ M, while the concentration of the complexes ranged from 0 to 23.8 μ M. The percentage of DMSO was 10%. Flow times were measured with a digital stopwatch. Each sample was measured in triplicate, and an average flow time was calculated. The data obtained are presented as $Ru([\text{complex}]/[\text{DNA}])$ versus $(\eta/\eta_0)^{1/3}$, where η is the relative viscosity of DNA in the presence of the compounds and η_0 is the relative viscosity of DNA.

3.7.2. Competitive Trials with Hoechst 33258

The Hoechst 33258 displacement test was performed by measuring the fluorescence extinction of the adduct CT-DNA (96.3 μ M)—Hoechst (5.3 μ M) in buffer (5.0 mM Tris-HCl, 0.5 mM NaOH, 50 mM NaCl) at pH 7.4. The emission intensity of the CT-DNA-Hoechst adduct at 485 nm (excitation wavelength of 340 nm) was monitored using $R(\text{II})/\text{complexes}$ as suppressors in different concentrations ranging from 0 to 210 μ M in DMSO. The percentage of DMSO used in the experiment was 5%. The fluorescence spectra were recorded from 300 to 500 nm, in triplicate, using an opaque 96-well plate at different temperatures (298 and 310 K). Data analysis was performed in a qualitative manner.

4. Conclusions

In this work, four new nitrosyl amino acid ruthenium complexes, $[\text{RuCl}(\text{NO})(\text{Gly-H})(\text{dppb})]\text{PF}_6$ (**1**), $[\text{RuCl}(\text{NO})(\text{Ala-H})(\text{dppb})]\text{PF}_6$ (**2**), $[\text{RuCl}(\text{NO})(\text{Phe-H})(\text{dppb})]\text{PF}_6$ (**3**) and $[\text{RuCl}(\text{NO})(\text{Val-H})(\text{dppb})]\text{PF}_6$ (**4**), were synthesized and characterized. The IR data indicate that the NO groups of complexes are true of the $\{\text{Ru}(\text{II})\text{-NO}^+\}$ type. The IR spectra also confirm the presence of amino acid ligands coordinated to the metal in a chelate (N-O) mode. The X-ray crystallographic data of complexes (**1**) and (**3**) confirm this statement. In vitro evaluation of these nitrosyl complexes revealed cytotoxic activity against the MDA-MB-231 (breast cancer) cells, and showed that in this case, the complexes are more sensitive to breast cancer cells than non-tumor cells (L929). All the compounds decreased the percentage of viable cells, and induced cell death by apoptosis. Complexes (**1–4**) inhibited the migration capacity of MDA-MB-231 cells, meaning they can be considered promising antimetastatic agents to be further explored as a possible anticancer drug. The compounds showed interaction with DNA via minor grooves, and displayed affinity to the HSA molecule.

Supplementary Materials: The following supporting information can be downloaded at: <https://www.mdpi.com/article/10.3390/inorganics11070270/s1>, Figure S1: $^{31}\text{P}\{^1\text{H}\}$ NMR spectrum for **1**, in $\text{CH}_2\text{Cl}_2/\text{D}_2\text{O}$ at 298K; Figure S2: $^{31}\text{P}\{^1\text{H}\}$ NMR spectrum for **2**, in $\text{CH}_2\text{Cl}_2/\text{D}_2\text{O}$ at 298K; Figure S3: $^{31}\text{P}\{^1\text{H}\}$ NMR spectrum for **3**, in $\text{CH}_2\text{Cl}_2/\text{D}_2\text{O}$ at 298K; Figure S4: $^{31}\text{P}\{^1\text{H}\}$ NMR spectrum for **4**, in $\text{CH}_2\text{Cl}_2/\text{D}_2\text{O}$ at 298K; Figure S5: ^1H NMR spectrum for **1**, in CDCl_3 ; Figure S6: ^1H NMR spectrum for **2**, in CDCl_3 ; Figure S7: ^1H NMR spectrum for **3**, in CDCl_3 ; Figure S8: ^1H NMR spectrum for **4**, in CDCl_3 ; Figure S9: $^{13}\text{C}\{^1\text{H}\}$ NMR spectrum for **1**, in CDCl_3 ; Figure S10: $^{13}\text{C}\{^1\text{H}\}$ NMR spectrum for **2**, in CDCl_3 ; Figure S11: $^{13}\text{C}\{^1\text{H}\}$ NMR spectrum for **3**, in CDCl_3 ; Figure S12: $^{13}\text{C}\{^1\text{H}\}$ NMR spectrum for **4**, in CDCl_3 ; Figure S13: Infrared spectrum for **1**, in KBr pallet; Figure S14: Infrared spectrum for **2**, in KBr pallet; Figure S15: Infrared spectrum for **3**, in KBr pallet; Figure S16: Infrared spectrum for **4**, in KBr pallet; Figure S17: UV-Vis spectrum for **1**, in CH_2Cl_2 ; Figure S18: UV-Vis spectrum for **2**, in CH_2Cl_2 ; Figure S19: UV-Vis spectrum for **3**, in CH_2Cl_2 ; Figure S20: UV-Vis spectrum for **4**, in CH_2Cl_2 ; Figure S21: Stern–Volmer plots for the quenching of HSA fluorescence by (A) $[\text{RuCl}(\text{NO})(\text{Ala})(\text{dppb})]\text{PF}_6$, (B) $[\text{RuCl}(\text{NO})(\text{Phe})(\text{dppb})]\text{PF}_6$ and (C) $[\text{RuCl}(\text{NO})(\text{Val})(\text{dppb})]\text{PF}_6$; Figure S22: Fluorescence spectrum of (A) HSA + $[\text{RuCl}(\text{NO})(\text{Ala})(\text{dppb})]\text{PF}_6$, (B) HSA + $[\text{RuCl}(\text{NO})(\text{Phe})(\text{dppb})]\text{PF}_6$ and (C) HSA + $[\text{RuCl}(\text{NO})(\text{Val})(\text{dppb})]\text{PF}_6$. Concentration da HSA = $5.0 \mu\text{mol L}^{-1}$, $\lambda_{\text{ex.}} = 280 \text{ nm}$, $\text{pH} = 7.4$ e $T = 298 \text{ K}$; Figure S23: Plot of $\log[(F_0 - F)/F]$ vs. $\log[Q]$: (A) $[\text{RuCl}(\text{NO})(\text{Gly})(\text{dppb})]\text{PF}_6$; (B) $[\text{RuCl}(\text{NO})(\text{Ala})(\text{dppb})]\text{PF}_6$, (C) $[\text{RuCl}(\text{NO})(\text{Phe})(\text{dppb})]\text{PF}_6$ and (D) $[\text{RuCl}(\text{NO})(\text{Val})(\text{dppb})]\text{PF}_6$; Figure S24: $^{31}\text{P}\{^1\text{H}\}$ NMR spectrum for **1**, in $\text{DMSO}-d_6$; Figure S25: $^{31}\text{P}\{^1\text{H}\}$ NMR spectrum for **2**, in $\text{DMSO}-d_6$; Figure S26: $^{31}\text{P}\{^1\text{H}\}$ NMR spectrum for **3**, in $\text{DMSO}-d_6$; Figure S27: $^{31}\text{P}\{^1\text{H}\}$ NMR (using an external capillary with D_2O), compound (**1**), $\text{DMSO}/\text{DMEM}/\text{GSH}$ solution 1:1:5. (Time: 0, 6, 24, 48 and 72 h); Figure S28: $^{31}\text{P}\{^1\text{H}\}$ NMR (using an external capillary with D_2O), compound (**4**), $\text{DMSO}/\text{DMEM}/\text{GSH}$ solution 1:1:5. (Time: 0, 6, 24, 48 and 72 h).

Author Contributions: Conceptualization, A.A.B.; methodology, M.I.F.B.; validation, A.C.D. and E.P.S.-L.; investigation, R.S.C., A.P.M.G., A.M.G., F.M.A., C.M.L., J.E. and H.V.R.; writing—original draft preparation, M.I.F.B. and A.C.D.; supervision, A.A.B. All authors have read and agreed to the published version of the manuscript.

Funding: This research was funded by FAPESP (grants 2022/11924-8, 2020/14561-8 and 2017/15850-0), CNPq (302844/2022-8), CAPES, FAPEMIG and RQ/MG. R.S.C. would like to thank the financial support provided by PROPP/UFOP, FAPEMIG (APQ-01674-18), and CNPq (grants 403588/2016-2 and 308370/2017-1).

Data Availability Statement: Crystallographic data were deposited at the Cambridge Crystallographic Data Centre as a supplementary publication (CCDC 1998258 for complex **1**, CCDC 1998259 for complex **3**). Copies of the data can be obtained, free of charge via www.ccdc.cam.ac.uk/conts/retrieving.html (accessed on 5 May 2023) (or from the Cambridge Crystallographic Data Centre, CCDC, 12 Union Road, Cambridge CB2 1EZ, UK; fax: +44-1223-336033; or e-mail: deposit@ccdc.cam.ac.uk).

Acknowledgments: The authors thank Dinorah Gambino for the invitation.

Conflicts of Interest: The authors declare no conflict of interest.

References

1. Riccardi, C.; Piccolo, M. Metal-Based Complexes in Cancer. *Int. J. Mol. Sci.* **2023**, *24*, 7289. [[CrossRef](#)] [[PubMed](#)]
2. Banerjee, S.; Banerjee, S. Metal-Based Complexes as Potential Anti-cancer Agents. *Anti-Cancer Agents Med. Chem.* **2022**, *22*, 2684–2707. [[CrossRef](#)] [[PubMed](#)]
3. Gamberi, T.; Hanif, M. Metal-Based Complexes in Cancer Treatment. *Biomedicines* **2022**, *10*, 2573. [[CrossRef](#)] [[PubMed](#)]
4. Ghosh, S. Cisplatin: The first metal based anticancer drug. *Bioorg. Chem.* **2019**, *88*, 102925. [[CrossRef](#)] [[PubMed](#)]
5. Coleman, J.; Sjoberg, D.D.; Demac, Q.; Odea, C.; McGill, M.; Tracey, A.; Nogueira, L.; Vickers, A.; Estes, C.; Fine, S.; et al. Phase 2b trial results of padeliporfin (WST11 or Tookad) vascular-targeted photodynamic therapy for partial gland ablation in men with intermediate-risk prostate cancer. *J. Clin. Oncol.* **2021**, *39*, e17006. [[CrossRef](#)]
6. Thota, S.; Rodrigues, D.A.; Crans, D.C.; Barreiro, E.J. Ru(II) Compounds: Next-Generation Anticancer Metallotherapeutics? *J. Med. Chem.* **2018**, *61*, 5805–5821. [[CrossRef](#)]
7. Coverdale, J.P.C.; Laroiya-McCarron, T.; Romero-Canelón, I. Designing Ruthenium Anticancer Drugs: What Have We Learnt from the Key Drug Candidates? *Inorganics* **2019**, *7*, 31. [[CrossRef](#)]
8. Murray, B.S.; Dyson, P.J. Recent progress in the development of organometallics for the treatment of cancer. *Curr. Opin. Chem. Biol.* **2020**, *56*, 28–34. [[CrossRef](#)]

9. Lee, S.Y.; Kim, C.Y.; Nam, T.-G. Ruthenium Complexes as Anticancer Agents: A Brief History and Perspectives. *Drug Des. Dev. Ther.* **2020**, *14*, 5375–5392. [[CrossRef](#)]
10. Riccardi, C.; Musumeci, D.; Capuozzo, A.; Irace, C.; King, S.; Krauss, I.R.; Paduano, L.; Montesarchio, D. “Dressing up” an Old Drug: An Aminoacyl Lipid for the Functionalization of Ru(III)-Based Anticancer Agents. *ACS Biomater. Sci. Eng.* **2018**, *4*, 163–174. [[CrossRef](#)]
11. Leite, C.M.; de Araujo-Neto, J.H.; Corrêa, R.S.; Colina-Vegas, L.; Martínez-Otero, D.; Martins, P.R.; Silva, C.G.; Batista, A.A. On the Cytotoxicity of Chiral Ruthenium Complexes Containing Sulfur Amino Acids against Breast Tumor Cells (MDA-231 and MCF-7). *Anti-Cancer Agents Med. Chem.* **2021**, *21*, 1172–1182. [[CrossRef](#)] [[PubMed](#)]
12. Golfeto, C.C.; Von Poelhsitz, G.; Selistre-De-Araújo, H.S.; de Araujo, M.P.; Ellena, J.; Castellano, E.E.; Lopes, L.G.; Moreira, I.S.; Batista, A.A. Synthesis, characterization and cytotoxic activities of the [RuCl₂(NO)(dppp)(L)]PF₆ complexes. *J. Inorg. Biochem.* **2010**, *104*, 489–495. [[CrossRef](#)] [[PubMed](#)]
13. Gaspari, A.P.; da Silva, R.S.; Carneiro, Z.A.; de Carvalho, M.R.; Carvalho, I.; Pernomian, L.; Ferreira, L.P.; Ramos, L.C.; de Souza, G.A.; Formiga, A.L. Improving Cytotoxicity against Breast Cancer Cells by Using Mixed-Ligand Ruthenium(II) Complexes of 2,2'-Bipyridine, Amino Acid, and Nitric Oxide Derivatives as Potential Anticancer Agents. *Anti-Cancer Agents Med. Chem.* **2021**, *21*, 1602–1611. [[CrossRef](#)]
14. Mello-Andrade, F.; Guedes, A.P.; Pires, W.C.; Velozo-Sá, V.S.; Delmond, K.A.; Mendes, D.; Molina, M.S.; Matuda, L.; de Sousa, M.A.M.; Melo-Reis, P.; et al. Ru(II)/amino acid complexes inhibit the progression of breast cancer cells through multiple mechanism-induced apoptosis. *J. Inorg. Biochem.* **2022**, *226*, 111625. [[CrossRef](#)] [[PubMed](#)]
15. Heinrich, T.A.; Von Poelhsitz, G.; Reis, R.I.; Castellano, E.E.; Neves, A.; Lanznaster, M.; Machado, S.P.; Batista, A.A.; Costa-Neto, C.M. A new nitrosyl ruthenium complex: Synthesis, chemical characterization, in vitro and in vivo antitumor activities and probable mechanism of action. *Eur. J. Med. Chem.* **2011**, *46*, 3616–3622. [[CrossRef](#)]
16. Dai, X.; Cheng, H.; Bai, Z.; Li, J. Breast Cancer Cell Line Classification and Its Relevance with Breast Tumor Subtyping. *J. Cancer* **2017**, *8*, 3131–3141. [[CrossRef](#)]
17. Batista, A.A.; Wohnrath, K.; Pereira, C.; Gambardella, M.T.P. Synthesis and characterization of the mer-[RuCl₃(NO)(dppb)] isomer. X-ray structures of fac-[RuCl₃(NO)(dppm)], cis-[RuCl₂(dppm)₂] and mer-[RuCl₃(NO)(dppb)] [dppm = 1,2-bis(diphenylphosphino)methane and dppb = 1,4-bis(diphenylphosphino)butane]. *Polyhedron* **1999**, *18*, 2079–2083. [[CrossRef](#)]
18. Almeida, M.A.P.; Nascimento, F.B.D.; Graminha, A.E.; Ferreira, A.G.; Ellena, J.; Mello, F.M.D.S.; de Lima, A.P.; Silveira-Lacerda, E.D.P.; Batista, A.A. Structural features and cytotoxic activities of [Ru(AA-H)(dppb)(bipy)]PF₆ complexes. *Polyhedron* **2014**, *81*, 735–742. [[CrossRef](#)]
19. Ghosh, K.; Kumar, S.; Kumar, R. Donation and scavenging of nitric oxide (NO) by flipping of the denticity of carboxylate ligand in novel ruthenium complexes: Photolability of the coordinated NO. *Inorg. Chim. Acta* **2013**, *405*, 24–30. [[CrossRef](#)]
20. Schultz, A.J.; Henry, R.L.; Reed, J.; Eisenberg, R. Crystal and molecular structure of trichloronitrosylbis(methyldiphenylphosphine) ruthenium(II), RuCl₃(NO)(PMePH₂)₂. *Inorg. Chem.* **1974**, *13*, 732–736. [[CrossRef](#)]
21. Zangl, A.; Klüfers, P.; Schaniel, D.; Woike, T. Photoinduced linkage isomerism of {RuNO}₆ complexes with bioligands and related chelators. *Dalton Trans.* **2009**, 1034–1045. [[CrossRef](#)] [[PubMed](#)]
22. Wang, H.; Onozuka, T.; Tomizawa, H.; Tanaka, M.; Miki, E. The unexpected reactions of [RuCl₃(2mqn)NO]– (H₂mqn=2-methyl-8-quinolinol) with 2-chloro-8-quinolinol (H₂cqn) and of [RuCl(2cqn)(2mqn)NO] on photoirradiation. *Inorg. Chim. Acta* **2004**, *357*, 1303–1308. [[CrossRef](#)]
23. Michael, D.; Mingos, P.; Sherman, D.J. Transition Metal Nitrosyl Complexes. In *Advances in Inorganic Chemistry*; Academic Press: Cambridge, MA, USA, 1989; Volume 34, pp. 293–377. [[CrossRef](#)]
24. Amaral, M.L.M.D.; Nascimento, R.D.; Silva, L.F.; Arantes, E.C.d.S.; Graminha, A.E.; da Silva, R.S.; Ueno, L.T.; Bogado, A.L.; DeFreitas-Silva, G.; de Lima, R.G. New trans-[Ru(NO)(NO₂)(dppb)(o-bdqi)]⁺ complex as NO donor encapsulated Pluronic F-127 micelles. *Polyhedron* **2022**, *218*, 115770. [[CrossRef](#)]
25. Lewandowska, H. Spectroscopic Characterization of Nitrosyl Complexes. In *Nitrosyl Complexes in Inorganic Chemistry, Biochemistry and Medicine I*; Structure and Bonding; Springer: Berlin/Heidelberg, Germany, 2013; pp. 115–165. [[CrossRef](#)]
26. De La Cruz, C.; Sheppard, N. A structure-based analysis of the vibrational spectra of nitrosyl ligands in transition-metal coordination complexes and clusters. *Spectrochim. Acta A Mol. Biomol. Spectrosc.* **2011**, *78*, 7–28. [[CrossRef](#)] [[PubMed](#)]
27. Mondal, B.; Paul, H.; Puranik, V.G.; Lahiri, G.K. Ruthenium mononitro and mononitroso terpyridine complexes incorporating azoimine based ancillary ligands. Synthesis, crystal structure, spectroelectrochemical properties and kinetic aspects. *J. Chem. Soc. Dalton Trans.* **2001**, 481–487. [[CrossRef](#)]
28. Santos, E.R.; Graminha, A.E.; Schultz, M.S.; Correia, I.; Selistre-de-Araújo, H.S.; Corrêa, R.S.; Ellena, J.; Lacerda, E.P.S.; Pessoa, J.C.; Batista, A.A. Cytotoxic activity and structural features of Ru(II)/phosphine/amino acid complexes. *J. Inorg. Biochem.* **2018**, *182*, 48–60. [[CrossRef](#)]
29. Rathgeb, A.; Böhm, A.; Novak, M.S.; Gavriluta, A.; Dömötör, O.; Tommasino, J.B.; Enyedy, É.A.; Shova, S.; Meier, S.; Jakupec, M.A.; et al. Ruthenium-Nitrosyl Complexes with Glycine, L-Alanine, L-Valine, L-Proline, D-Proline, L-Serine, L-Threonine, and L-Tyrosine: Synthesis, X-ray Diffraction Structures, Spectroscopic and Electrochemical Properties, and Antiproliferative Activity. *Inorg. Chem.* **2014**, *53*, 2718–2729. [[CrossRef](#)]

30. Kalaivani, P.; Saranya, S.; Poornima, P.; Prabhakaran, R.; Dallemer, F.; Padma, V.V.; Natarajan, K. Biological evaluation of new nickel(II) metallates: Synthesis, DNA/protein binding and mitochondrial mediated apoptosis in human lung cancer cells (A549) via ROS hypergeneration and depletion of cellular antioxidant pool. *Eur. J. Med. Chem.* **2014**, *82*, 584–599. [[CrossRef](#)]
31. Kratz, F. A clinical update of using albumin as a drug vehicle—A commentary. *J. Control. Release* **2014**, *190*, 331–336. [[CrossRef](#)]
32. Lakowicz, J.R. *Principles of Fluorescence Spectroscopy*; Springer: Boston, MA, USA, 2006; Volume 4, pp. 853–954, ISBN 978-0-387-46312.
33. Silva, H.V.R.; Dias, J.S.M.; da Silva, G.F.; Vegas, L.C.; Ionta, M.; Corrêa, C.C.; Batista, A.A.; Barbosa, M.I.F.; Doriguetto, A.C. Phosphine/diimine ruthenium complexes with Cl^- , CO, NO^+ , NO_2^- , NO_3^- and pyridine ligands: Pro-apoptotic activity on triple-negative breast cancer cells and DNA/HSA interactions. *Polyhedron* **2018**, *144*, 55–65. [[CrossRef](#)]
34. Ramadevi, P.; Singh, R.; Jana, S.S.; Devkar, R.; Chakraborty, D. Ruthenium complexes of ferrocene mannich bases: DNA/BSA interactions and cytotoxicity against A549 cell line. *J. Photochem. Photobiol. A Chem.* **2015**, *305*, 1–10. [[CrossRef](#)]
35. Beckford, F.; Thessing, J.; Woods, J.; Didion, J.; Gerasimchuk, N.; Gonzalez-Sarrias, A.; Seeram, N.P. Synthesis and structure of $[(\eta^6\text{-p-cymene})\text{Ru}(2\text{-anthracen-9-ylmethylene-N-ethylhydrazinecarbothioamide})\text{Cl}]\text{Cl}$; biological evaluation, topoisomerase II inhibition and reaction with DNA and human serum albumin. *Metallomics* **2011**, *3*, 491–502. [[CrossRef](#)] [[PubMed](#)]
36. Cacita, N.; Nikolaou, S. Studying the interaction between trinuclear ruthenium complexes and human serum albumin by means of fluorescence quenching. *J. Lumin.* **2016**, *169*, 115–120. [[CrossRef](#)]
37. Ross, P.D.; Subramanian, S. Thermodynamics of protein association reactions: Forces contributing to stability. *Biochemistry* **1981**, *20*, 3096–3102. [[CrossRef](#)] [[PubMed](#)]
38. Riccardi, C.; Piccolo, M.; Ferraro, M.G.; Graziano, R.; Musumeci, D.; Trifuoggi, M.; Irace, C.; Montesarchio, D. Bioengineered lipophilic Ru(III) complexes as potential anticancer agents. *Biomater. Adv.* **2022**, *139*, 213016. [[CrossRef](#)] [[PubMed](#)]
39. Martínez, A.; Suárez, J.; Shand, T.; Magliozzo, R.S.; Sánchez-Delgado, R.A. Interactions of arene–Ru(II)–chloroquine complexes of known antimalarial and antitumor activity with human serum albumin (HSA) and transferrin. *J. Inorg. Biochem.* **2011**, *105*, 39–45. [[CrossRef](#)]
40. Tan, C.; Liu, J.; Li, H.; Zheng, W.; Shi, S.; Chen, L.; Ji, L. Differences in structure, physiological stability, electrochemistry, cytotoxicity, DNA and protein binding properties between two Ru(III) complexes. *J. Inorg. Biochem.* **2008**, *102*, 347–358. [[CrossRef](#)]
41. Pages, B.J.; Ang, D.L.; Wright, E.P.; Aldrich-Wright, J.R. Metal complex interactions with DNA. *Dalton Trans.* **2015**, *44*, 3505–3526. [[CrossRef](#)]
42. Barra, C.V.; Netto, A.V.G. Antitumour Complexes and DNA Interactions and their Tools of Analysis: An Approach to Metalintercalators. *Rev. Virtual Quim.* **2015**, *7*, 1998–2016. [[CrossRef](#)]
43. Wheate, N.J.; Brodie, C.R.; Collins, J.G.; Kemp, S.; Aldrich-Wright, J.R. DNA Intercalators in Cancer Therapy: Organic and Inorganic Drugs and Their Spectroscopic Tools of Analysis. *Mini-Rev. Med. Chem.* **2007**, *7*, 627–648. [[CrossRef](#)]
44. Biver, T.; García, B.; Leal, J.M.; Secco, F.; Turriani, E. Left-handed DNA: Intercalation of the cyanine thiazole orange and structural changes. A kinetic and thermodynamic approach. *Phys. Chem. Chem. Phys.* **2010**, *12*, 13309–13317. [[CrossRef](#)]
45. Saito, M.; Kobayashi, M.; Iwabuchi, S.-I.; Morita, Y.; Takamura, Y.; Tamiya, E. DNA Condensation Monitoring after Interaction with Hoechst 33258 by Atomic Force Microscopy and Fluorescence Spectroscopy. *J. Biochem.* **2004**, *136*, 813–823. [[CrossRef](#)] [[PubMed](#)]
46. Guan, Y.; Zhou, W.; Yao, X.; Zhao, M.; Li, Y. Determination of nucleic acids based on the fluorescence quenching of Hoechst 33258 at pH 4.5. *Anal. Chim. Acta* **2006**, *570*, 21–28. [[CrossRef](#)]
47. Souza, M.L.; Roveda, A.C., Jr.; Pereira, J.C.M.; Franco, D.W. New perspectives on the reactions of metal nitrosyls with thiolates as nucleophiles. *Coord. Chem. Rev.* **2016**, *306*, 615–627. [[CrossRef](#)]
48. Roncaroli, F.; Olabe, J.A. The Reactions of Nitrosyl Complexes with Cysteine. *Inorg. Chem.* **2005**, *44*, 4719–4727. [[CrossRef](#)]
49. Otwinowski, Z.; Minor, W. HKL Denzo and Scalepack. In *Methods in Enzymology*; Carter, C.W., Jr., Sweet, R.M., Eds.; Academic Press: New York, NY, USA, 1997; Volume 276, pp. 307–326.
50. Sheldrick, G.M. Crystal structure refinement with SHELXL. *Acta Crystallogr. Sect. C Struct. Chem.* **2015**, *71*, 3–8. [[CrossRef](#)] [[PubMed](#)]
51. Coppens, P.; Leiserowitz, L.; Rabinovich, D. Calculation of absorption corrections for camera and diffractometer data. *Acta Crystallogr.* **1965**, *18*, 1035–1038. [[CrossRef](#)]
52. Farrugia, L.J. ORTEP-3 for Windows—A version of ORTEP-III with a Graphical User Interface (GUI). *J. Appl. Crystallogr.* **1997**, *30*, 565. [[CrossRef](#)]
53. Mosmann, T. Rapid colorimetric assay for cellular growth and survival: Application to proliferation and cytotoxicity assays. *J. Immunol. Methods* **1983**, *65*, 55–63. [[CrossRef](#)]
54. Bronikowska, J.; Szliszka, E.; Jaworska, D.; Czuba, Z.P.; Krol, W. The Coumarin Psoralidin Enhances Anticancer Effect of Tumor Necrosis Factor-Related Apoptosis-Inducing Ligand (TRAIL). *Molecules* **2012**, *17*, 6449–6464. [[CrossRef](#)]
55. Rahman, S.N.S.A.; Wahab, N.A.; Malek, S.N.A. In Vitro Morphological Assessment of Apoptosis Induced by Antiproliferative Constituents from the Rhizomes of Curcuma zedoaria. *Evid.-Based Complement. Altern. Med.* **2013**, *2013*, 257108. [[CrossRef](#)]

56. Rogalska, A.; Marczak, A.; Gajek, A.; Szwed, M.; Śliwińska, A.; Drzewoski, J.; Józwiak, Z. Induction of apoptosis in human ovarian cancer cells by new anticancer compounds, epothilone A and B. *Toxicol. In Vitro* **2013**, *27*, 239–249. [[CrossRef](#)] [[PubMed](#)]
57. Chatterjee, T.; Pal, A.; Dey, S.; Chatterjee, B.K.; Chakrabarti, P. Interaction of Virstatin with Human Serum Albumin: Spectroscopic Analysis and Molecular Modeling. *PLoS ONE* **2012**, *7*, e37468. [[CrossRef](#)] [[PubMed](#)]

Disclaimer/Publisher's Note: The statements, opinions and data contained in all publications are solely those of the individual author(s) and contributor(s) and not of MDPI and/or the editor(s). MDPI and/or the editor(s) disclaim responsibility for any injury to people or property resulting from any ideas, methods, instructions or products referred to in the content.